

Effects of metallicity, star formation conditions and evolution in B and Be stars.

I: Large Magellanic Cloud, field of NGC 2004.

C. Martayan¹, Y. Frémat², A.-M. Hubert¹, M. Floquet¹, J. Zorec³, and C. Neiner^{1,4}

¹ GEPI, UMR 8111 du CNRS, Observatoire de Paris-Meudon, 92195 Meudon Cedex, France

² Royal Observatory of Belgium, 3 avenue circulaire, 1180 Brussels, Belgium

³ Institut d'Astrophysique de Paris (IAP), 98bis boulevard Arago, 75014 Paris, France

⁴ Instituut voor Sterrenkunde, KU Leuven, Celestijnenlaan 200B, 3001 Belgium

Received /Accepted

Abstract. Spectroscopic observations of hot stars belonging to the young cluster LMC-NGC 2004 and its surrounding region were carried out with the VLT-GIRAFFE facilities in MEDUSA mode. We determine fundamental parameters (T_{eff} , $\log g$, $V \sin i$, and radial velocity), for all B and Be stars in the sample thanks to a code developed in our group. The effect of fast rotation (stellar flattening and gravitational darkening) are taken into account in this study. We also determine the age of observed clusters. We compare the mean $V \sin i$ obtained for field and cluster B and Be stars in the Large Magellanic Cloud (LMC) with the ones in the Milky Way (MW). We find, in particular, that Be stars rotate faster in the LMC than in the MW, in the field as well as in clusters. We discuss the relations between $V \sin i$, metallicity, star formation conditions and stellar evolution by comparing the LMC with the MW. We conclude that Be stars begin their Main Sequence life with an initial rotational velocity higher than the one of B stars. It is probable that only part of the B stars, with a sufficient initial rotational velocity, can become Be stars. This result may explain the differences in the proportion of Be stars in clusters with similar ages.

Key words. Stars: early-type – Stars: emission-line, Be – Galaxies: Magellanic Clouds – Stars: fundamental parameters – Stars: evolution – Stars: rotation

1. Introduction

The study of physical properties of B stars with respect to the relative frequency of Be stars in young open clusters and their surrounding field can provide important insights into the origin of the Be phenomenon. Indeed, our knowledge of mass-loss conditions, which lead to the formation of an anisotropic envelope around a fraction of B stars, is still very poor. Several physical processes could be involved, such as rapid rotation, non-radial pulsations, magnetic fields, evolutionary effects, binarity... Although the Be phenomenon has frequently been considered as a rapid rotation-related phenomenon in OB stars, it is not yet established whether only a fraction or all of the rapidly rotating early-type stars evolve into Be stars.

Several recent studies tackled the major question of the influence of metallicity and evolution on rapid rotators. The Be phenomenon could be favoured in stars of low metallicity (Maeder et al. 1999). Preliminary results by Royer et al. (2004) could confirm this metallicity effect, although they use limited stellar samples. The appearance of the Be phenomenon

could also depend on stellar ages (Fabregat & Torrejón 2000). Accounting for the effects of fast rotation and of gravitational darkening, Zorec et al. (2005) concluded that Be stars spread over the whole Main Sequence (MS) evolutionary phase. However, they find that in massive stars the Be phenomenon tends to be present at smaller $\frac{t}{t_{\text{MS}}}$ age ratios than in less massive stars. Moreover, Keller (2004) found that young clusters host more rapid rotators than their surrounding field. This assessment is valid for the LMC, as well as in the Galaxy. A similar trend was found by Gies & Huang (2004) from a spectroscopic survey of young galactic clusters.

Up to now, spectroscopic surveys were only obtained with a resolution power $R < 5000$ and/or a low signal to noise ratio (S/N). The new instrumentation FLAMES-GIRAFFE installed at the VLT-UT2 at ESO is particularly well suited to obtain high quality spectra of large samples needed for the study of stellar populations. Thus, we have undertaken the determination of fundamental parameters for a large sample of B and Be stars in regions of different metallicity: (i) to check whether the low metallicity favours the formation of rapid rotators and in particular of Be stars; and (ii) to investigate the evolutionary status of Be stars. In a first paper (Martayan et al. 2005,

Send offprint requests to: C. Martayan

Correspondence to: christophe.martayan@obspm.fr

hereafter Paper I), we reported the identification of numerous B-type stars, the discovery of new Be stars and spectroscopic binaries in the young cluster LMC-NGC 2004 and its surrounding field with the help of medium resolution spectra obtained with the FLAMES instrumentation. The present paper deals with fundamental parameters and evolutionary status of a very large fraction of those objects, taking into account rotational effects (stellar flattening, gravitational darkening) when appropriate.

2. Observations

This work makes use of spectra obtained with the multifibre spectrograph VLT-FLAMES in Medusa mode (132 fibres) at medium resolution ($R=6400$) in setup LR02 (396.4 - 456.7 nm). Observations (ESO runs 72.D-0245B and 73.D-0133A) were carried out in the young cluster LMC-NGC 2004 and in its surrounding field, as part of the Guaranteed Time Observation programmes of the Paris Observatory (P.I.: F. Hammer). The observed field (25' in diameter) is centered at $\alpha(2000) = 05^{\text{h}} 29^{\text{m}} 00^{\text{s}}$ and $\delta(2000) = -67^{\circ} 14' 00''$. Besides the young cluster NGC 2004, this field contains several high-density groups of stars (KMHK 943, 971, 963, 991, 988 and BSDL 2001). Spectra were obtained on November 24, 2003 and April 12, 2004; at these dates, the heliocentric velocities are smaller than 1.5 km s^{-1} . The strategy and conditions of observations, as well as the spectra reduction, are described in Paper I. A significant sample of the B stars population (168 objects), 6 O and 2 A stars were observed during the two observing runs. Since the V magnitude of the selected targets ranges from 13.7 to 17.8 mag, we chose a 2-hour integration time. This corresponds to an average S/N ≈ 120 , with individual values ranging from ~ 20 to ~ 150 for the fainter and brighter stars, respectively.

The colour diagram V versus B-V (Fig. 1), derived from our instrumental photometry, shows the B and Be stars in our sample compared to all the stars in the EIS-LMC 33 field. Several stars present a strong reddening and are mainly located either in the clusters NGC 2004, KMHK 943, KMHK 971, 'unknown2' and in the galactic open cluster HS 66325, either at the periphery of the H II region LHA 120-N51A, or in the field, but without explicit link between all these regions. The locations of the observed O, B and A-type stars are shown in the LMC 33 field from the EIS pre-FLAMES survey (Fig. 2).

Finally, among the 124812 stars which we have listed in the EIS LMC 33 field, our pre-selection with photometric criteria gives 1806 B-type stars. And we have observed 177 B-type stars among the 1235 B-type stars which are observable in the VLT-FLAMES/GIRAFFE field. The ratio of observed to observable B-type stars represents 14.3%. Consequently, this sample is statistically significant.

3. Fundamental parameters determination

One important step in the analysis of the data collected with FLAMES is the determination of the stellar fundamental parameters. In order to derive the effective temperature (T_{eff}), surface gravity ($\log g$), projected rotational velocity ($V \sin i$) and radial velocity (RV) in an homogeneous and coherent

Table 1. Atoms and ions treated in the computations assuming NLTE. The number of levels taken into account for each ion is given.

Atom	Ion	Number of levels
Hydrogen	H I	8 levels + 1 superlevel
	H II	1 level
Helium	He I	24 levels
	He II	20 levels
	He III	1 level
Carbon	C II	53 levels all individual levels
	C III	12 levels
	C IV	9 levels + 4 superlevels
	C V	1 level
Nitrogen	N I	13 levels
	N II	35 levels + 14 superlevels
	N III	11 levels
	N IV	1 level
Oxygen	O I	14 levels + 8 superlevels
	O II	36 levels + 12 superlevels
	O III	9 levels
	O IV	1 level
Magnesium	Mg II	21 levels + 4 superlevels
	Mg III	1 level

way for the whole stellar sample, we use the GIRFIT least squares procedure, which is able to handle large datasets and was previously developed and described by Frémat et al. (2005a). GIRFIT fits the observations with theoretical spectra interpolated in a grid of stellar fluxes computed with the SYNSPEC programme and from model atmospheres calculated with TLUSTY (Hubeny & Lanz 1995, see references therein) or/and with ATLAS9 (Kurucz 1993; Castelli et al. 1997). It accounts for the instrumental resolution through convolution of spectra with a Gaussian function and for Doppler broadening due to rotation. Use is made of subroutines taken from the ROTINS computer code provided with SYNSPEC (Hubeny & Lanz 1995).

It is worth noting that the spectra obtained in this way do not take into account the second order effects of fast rotation (stellar flattening and gravitational darkening), which are expected to be strong in Be stars. To introduce these effects in our discussion, stellar parameters are corrected afterwards by adopting a grid of synthetic stellar spectra computed by Frémat et al. (2005b) with the FASTROT computer code assuming a solid-body-type rotation. In the following sections, the terms 'apparent' and 'parent non-rotating counter-part' (pnrc) are used as defined by Frémat et al. (2005b).

We introduce in the following sections the grid of model atmospheres (Sect. 3.1) we use, the fitting criteria we adopt in the GIRFIT procedure (Sect. 3.2) and the corrections for fast rotation we apply on the Be stars' fundamental parameters (Sect. 3.4). The calibrations that allow us to estimate the spectral type of each non-Be target from the equivalent width of the hydrogen and helium lines are detailed in Sect. 3.3.

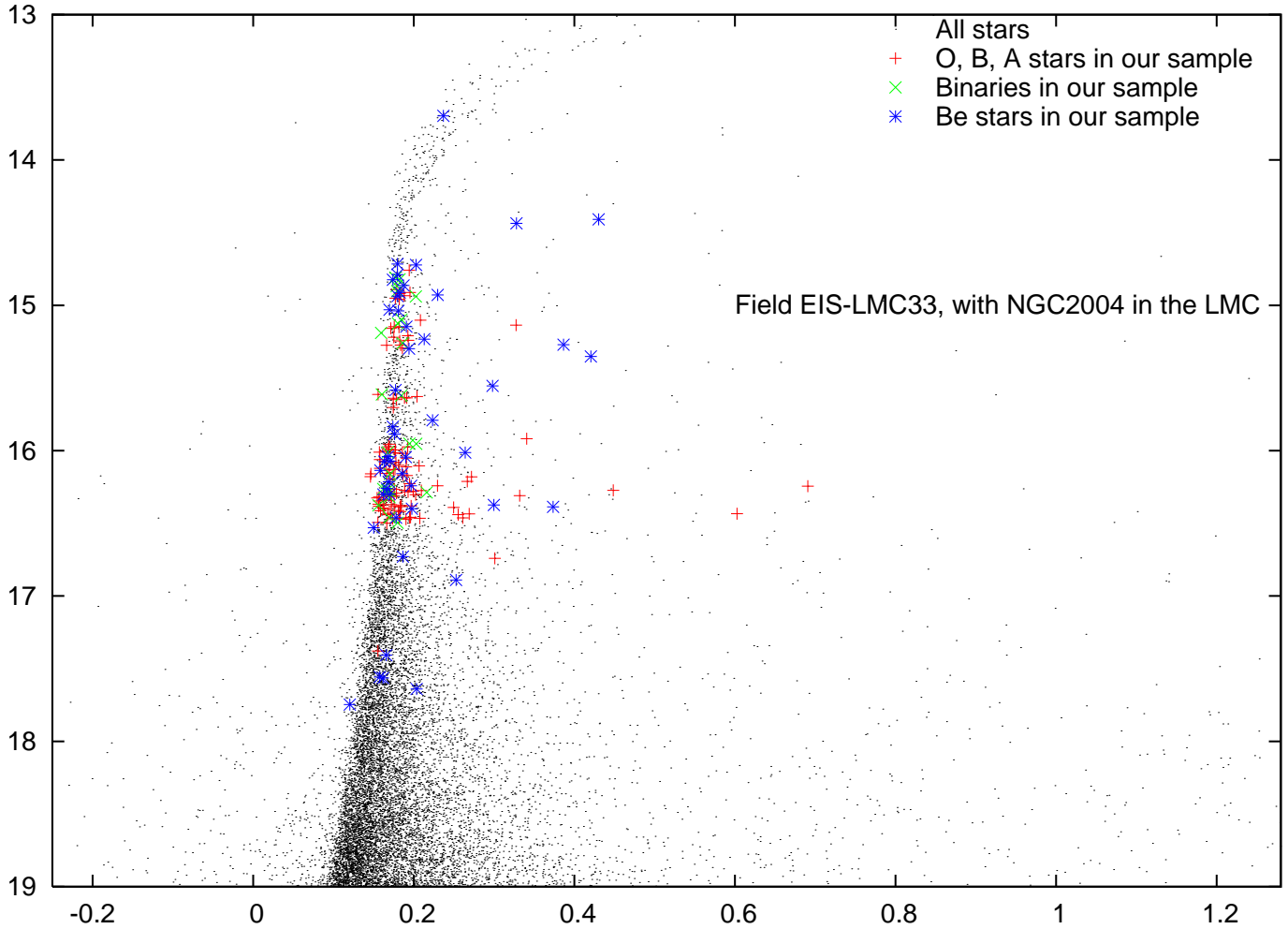


Fig. 1. Instrumental V versus instrumental (B-V) colour diagram from our photometry in the EIS LMC 33 field. The '.' symbols correspond to all stars in this field. '*' show the Be stars, '+' the O-B-A stars and 'x' the binaries in the sample. Several stars in this sample have a strong reddening, they are located mainly in clusters, and in the H II region LHA 120-N51A.

3.1. Grid of model atmospheres

The models we use to build the GIRFIT input grid of stellar fluxes are computed in two consecutive steps. To account in the most effective way for line-blanketing, the temperature structure of the atmospheres is computed using the ATLAS9 computer code (Kurucz 1993; Castelli et al. 1997). Non-LTE level populations are then estimated for each of the atoms we consider using TLUSTY (Hubeny & Lanz 1995) and keeping fixed the temperature and density distributions obtained with ATLAS9.

Table 1 lists the ions that are introduced in the computations. Except for C II, the atomic models we use in this work were downloaded from TLUSTY's homepage (<http://tlusty.gsfc.nasa.gov>) maintained by I. Hubeny and T. Lanz. C II is treated with the MODION IDL package developed by Varosi et al. (1995) and the atomic data (oscillator strengths, energy levels, and photoionization cross-sections) from the TOPBASE database (Cunto et al. 1993). It reproduces the results obtained by Sigut (1996).

In this way, and for each spectral region studied in the present work, the specific intensity grids are computed for ef-

fective temperatures and surface gravities ranging from 15000 K to 27000 K and from 2.5 to 5.0 dex, respectively. For $T_{\text{eff}} < 15000$ K and $T_{\text{eff}} > 27000$ K we use LTE calculations and the OSTAR 2002 NLTE model atmospheres grid (Lanz & Hubeny 2003), respectively.

The metallicities of the model atmospheres are chosen to be as close as possible to the NGC 2004 averaged value, $[m/H] = -0.45$ (where $[m/H] = \log(m/H)_{\text{LMC}} - \log(m/H)_{\odot}$), estimated from the results by Korn et al. (2002, Table 3). The Kurucz and OSTAR 2002 models we use are therefore those calculated for $[m/H] = -0.5$. Finally, the complete input flux grid is built assuming the averaged element abundances derived by Korn et al. (2002) for C, N, O, Mg, Si, and Fe. The other elements, except hydrogen and helium, are assumed to be underabundant by -0.45 dex relative to the Sun.

3.2. The GIRFIT procedure: fitting criteria and continuum level

The procedure we adopt to derive the stellar fundamental parameters mainly focuses on the spectral domain ranging from 4000 to 4500 Å, which gathers two hydrogen lines (H γ and

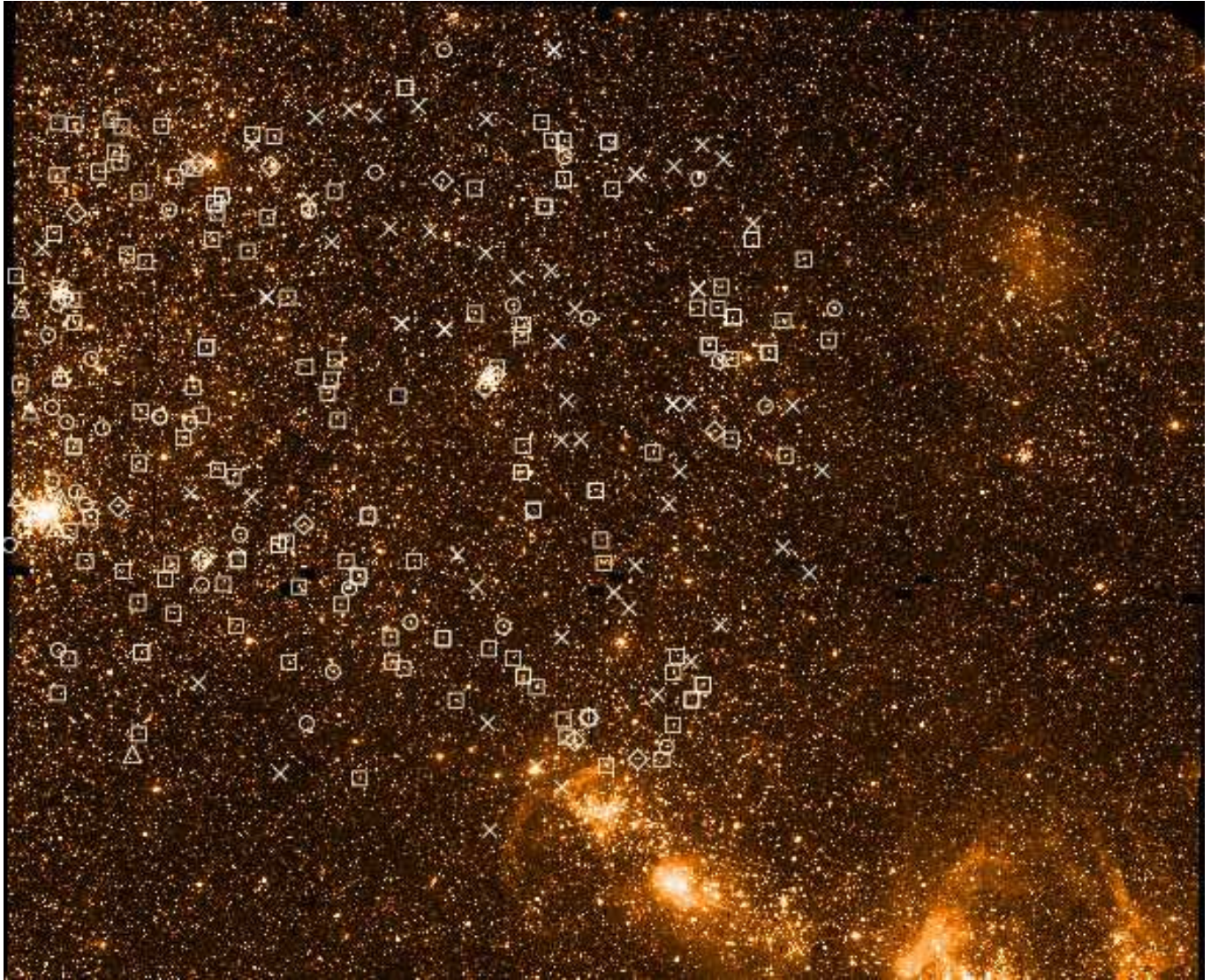


Fig. 2. The LMC 33 field from the EIS pre-FLAMES survey. Circles represent Be stars in the sample, squares O-B-A stars, and crosses sky fibres. Triangles and diamonds indicate Be and B stars with a strong reddening, respectively. In the southwest lies the H II region LHA 120-N51A.

H δ), 8 strong helium lines (He I λ 4009, 4026, 4121, 4144, 4169, 4388, 4471 and He II λ 4200) and several weak lines of silicon and carbon. The χ^2 parameter is computed on different spectral zones generally centred on these temperature- and gravity-sensitive diagnostic features. However, due to the moderate spectral resolution and frequent high apparent rotational velocities of targets, other criteria such as those based on silicon lines cannot be used. Furthermore it is worth noting that even the He I/H I line ratios used to estimate T_{eff} and $\log g$ values are less accurate for early B-type stars (B1-B0) than for later types, the simultaneous fit of several hydrogen and helium line-profiles enables us to obtain the sought stellar parameters quite easily, within the error boxes given in Table 2 (see also Fig. 1 in Frémat et al. 2005b). In the most dubious cases, the overall agreement between observed and synthetic spectra was checked over the complete spectral range.

In Be stars, which often display circumstellar emission/absorption in their spectra, the zones are further defined

to exclude any part of the spectral lines that could be deformed by line emission or shell absorption (e.g. hydrogen line cores). Note that, as the parameters derived for Be stars at this stage of the procedure do not take into account the effects of fast rotation (see Sect. 3.4), they will be further called apparent fundamental parameters.

During the spectra fitting procedure, 4 free parameters are considered: the effective temperature, the surface gravity, the projected rotational velocity and the radial velocity. To reduce as much as possible the impact of noise on the location of the stellar continuum, we also include a fifth parameter standing for the wavelength-independent ratio (i.e. a scaling factor) between the mean “flux” level of the normalized observed and theoretical spectra. Assuming a Poisson noise distribution to compute a reference spectrum, Fig. 3 shows how the derived fundamental parameters can be affected by a decrease of S/N, while Table 2 lists the averaged absolute errors on the fundamental parameters expected for different values of S/N.

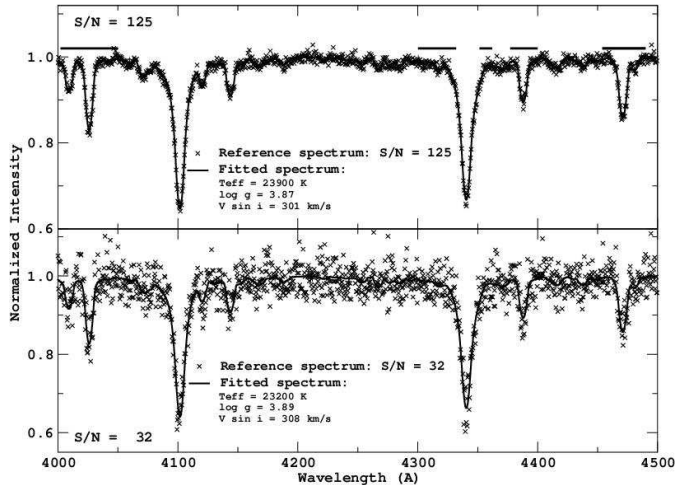


Fig. 3. Reference spectra (crosses) computed for $T_{\text{eff}} = 25000$ K, $\log g = 3.87$ and $V \sin i = 300$ km s $^{-1}$, for different S/N, are fitted using the GIRFIT procedure. The obtained fundamental parameters are noted on the figure.

For each star of the sample, we repeat the GIRFIT procedure several times with different fitted zones and initial parameters values in order to scan the complete space of solutions. The solutions we finally select are those with the lowest χ^2 re-computed over the same wavelength range: the whole spectrum for O, B, and A-type stars without emission, and only the blue part of the spectrum (4000–4250 Å) for Be stars in order to avoid, as much as possible, the influence of line emission in the hydrogen lines. After a final visual check of the adjusted spectra, the RV determinations obtained at the end of the GIRFIT procedure are compared to the values directly measured on the observations. If this ultimate verification is successful, the process stops. Otherwise, the fitting spectral zones are modified and the procedure is restarted. Examples of fitted spectra, for a B, an O-B and a Be star are given in Fig. 4.

Following Bouret et al. (2003), who used the same atomic data, there is no difference between fits obtained with TLUSTY-SYNSPEC (Hubeny & Lanz 1995) and with the CMFGEN code (Hillier & Miller 1998), which takes into account not only NLTE effects and line-blanketing but also a wind model with mass loss. This effect is present in O stars, but is not critical for B-type stars. Bouret et al. (2003) presented several fits for their sample of O and B stars and obtained similar apparent fundamental parameters with these two codes for early B-type stars. This study validates our choice of code for determining the fundamental parameters of B stars.

3.3. Spectral classification determination

The spectral type and luminosity class of the B-type stars we observed are determined in two different ways. First, we use an iterative method we developed, which has the advantage of being fast and easy to use. We estimate the spectral type from the equivalent width of the H γ line by assuming, in a first step, that our sample is only composed of dwarf stars. The spectral type is combined with the equivalent width of the He I 4471

line to derive, in a second step, the luminosity class, which is then used to rederive the spectral type. Several iterations are required to obtain a combination of spectral type/luminosity class fully coherent with the equivalent widths of the selected lines (H γ and He I 4471). The equivalent width calibrations we adopt in this procedure are those proposed by Azzopardi (1987) and Jaschek & Jaschek (1995) for H γ and by Didelon (1982) for the He I 4471 line.

Table 2. Averaged absolute errors on the fundamental parameters introduced by different S/N. For $V \sin i \leq 50$ km s $^{-1}$, the error is estimated to ± 20 km s $^{-1}$ (due to the intermediate resolution) and the minimum error in $V \sin i$ is ± 10 km s $^{-1}$ for the other cases.

S/N	$\Delta(T_{\text{eff}})$ (%)	$\Delta(\log g)$ (%)	$\Delta(V \sin i)$ (%)
30	20	10	30
40	15	10	20
50	12	10	16
60	10	9	16
70	8	8	10
80	6	6	10
90	6	6	7
100	5	5	5
120	5	5	5
>140	<5	<5	<5

The second method transcribes the set of fundamental parameters we derived by fitting the observed spectra into spectral type and luminosity class, with the help of effective temperature and surface gravity calibrations given by Gray & Corbally (1994) and Zorec (1986) for B stars, and by Bouret et al. (2003) for hotter stars.

The differences in the results provided by these two methods are, on average, half a spectral subtype and half a luminosity class for stars between B0 and B5, affecting both the equivalent width measurements and the derived stellar fundamental parameters. However, the first method fails to give a reliable spectral classification for the few hotter (late O) and cooler (B5-A0) stars in the sample. Moreover, for Be stars, the spectral classification determination is only performed using the derived apparent fundamental parameters (second method), since the emission contamination, often present in H γ and in several cases in the He I 4471 line, makes the first method particularly inappropriate for early Be stars.

3.4. Effects of fast rotation

As mentioned in the introduction, Be stars are fast rotators with angular velocities probably around 90% of their breakup velocity (Frémat et al. 2005b). It is further expected that solid-body-type fast rotation flattens the star, which causes a gravitational darkening of the stellar disk due to the variation of the temperature and density distribution from pole to equator. For Be stars, we therefore have to account for these effects

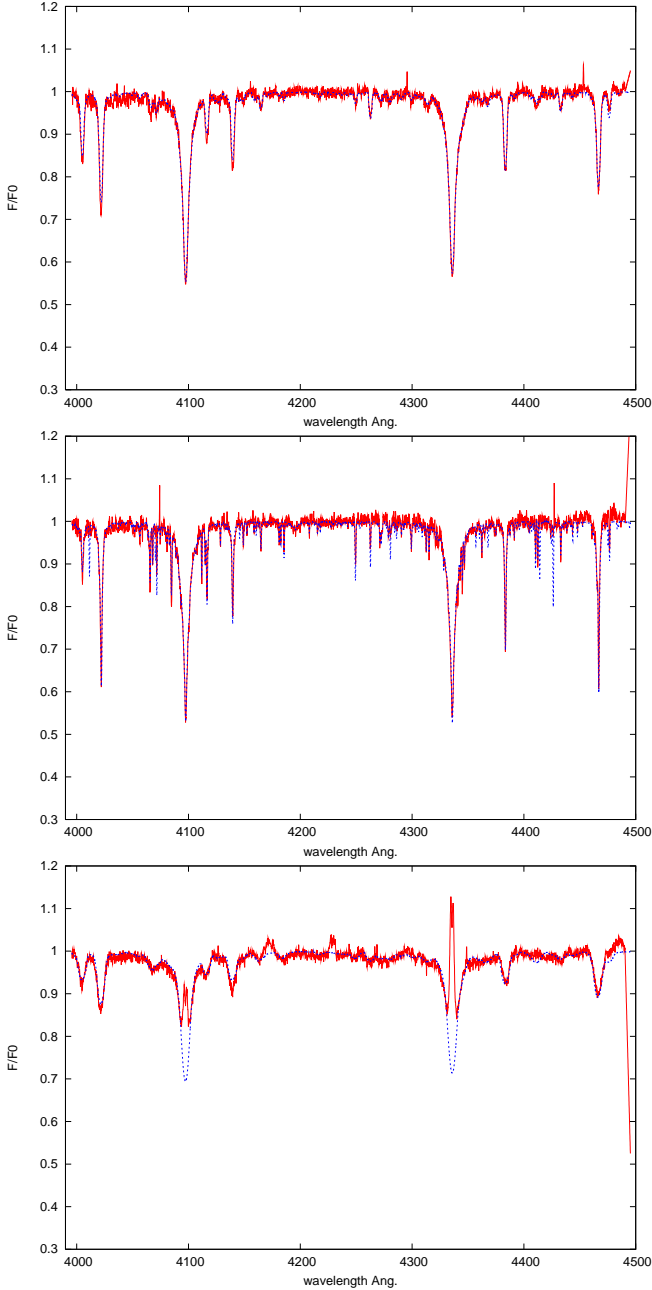


Fig. 4. Example of fits (dotted lines) of observed spectra (solid lines). Upper panel: The MHF119707 B star. The fit gives $T_{\text{eff}} = 21500$ K, $\log g = 3.6$ dex, $V \sin i = 134$ km s $^{-1}$, and $RV = 308$ km s $^{-1}$. Medium panel: The MHF67663 O-B star. The fit gives $T_{\text{eff}} = 29500$ K, $\log g = 4.3$ dex, $V \sin i = 9$ km s $^{-1}$, and $RV = 306$ km s $^{-1}$. Lower panel: The MHFBe136844 Be star. The fit gives $T_{\text{eff}} = 23000$ K, $\log g = 3.5$ dex, $V \sin i = 348$ km s $^{-1}$, and $RV = 315$ km s $^{-1}$.

on the stellar spectra and, consequently, on the determination of the fundamental parameters. In the present paper, these effects are introduced as corrections directly applied to the apparent fundamental parameters we derived. These corrections are computed by systematically comparing a grid of spectra taking into account the effects of fast rotation obtained with the FASTROT code for different values of pnr (i.e. parent non-

rotating counterpart) stellar parameters (T_{eff}^o , $\log g_o$, $V \sin i^{\text{true}}$) and of angular velocity (Ω/Ω_c , where Ω_c is the break-up angular velocity) to a grid of spectra computed using usual plane-parallel model atmospheres. Adopting the same spectroscopic criteria than those described in Section 3.2 (i.e. hydrogen and helium lines), we obtain different sets of pnr and apparent stellar parameters (T_{eff} , $\log g$, $V \sin i$). The corrections we apply to the apparent stellar parameters of the Be stars in the sample (Section 3.2) are interpolated in this grid using an iterative procedure. Generally, only a few iterations are needed (to reach differences smaller than 500 K for T_{eff} and 0.05 dex for $\log g$) to obtain the final pnr parameters for a given Ω/Ω_c . The radius, mass, and luminosity of the non-rotating stellar counterparts are estimated by (T_{eff}^o ; $\log g_o$)-interpolation in the theoretical evolutionary tracks (Charbonnel et al. 1993).

4. Results

In this section we present the results on stellar parameters and spectral classification determination we obtain as described in Sect. 3 for non-emission line O-B-A stars, for Be stars, and for some spectroscopic binary systems. The $\alpha(2000)$ and $\delta(2000)$ coordinates, the instrumental V magnitude and the instrumental (B-V) colour index for individual stars are extracted from EIS pre-FLAMES (LMC 33) survey images, as reported in Paper I. The S/N we measure in the spectra may differ for objects with the same magnitude depending either on the position of the fibres within the GIRAFFE field, either on transmission rate differences, or on the presence of clouds partly obscuring the observed field (the field of GIRAFFE has a 25' diameter on the sky). All these informations are given in Tables 3, 7, and 6 for the different groups of stars mentioned above, respectively.

4.1. O-B-A stars

4.1.1. Fundamental parameters of O-B-A stars

Early-type stars that do not show intrinsic emission lines in their spectrum and have not been detected as spectroscopic binaries are listed in Table 3 sorted by their MHF catalogue number. Moreover, three stars with a KWBBBe name, reported as Be stars by Keller et al. (1999) but not confirmed or in a temporary B phase at epochs of VLT/FLAMES observations, are added at the end of the Table. The fundamental parameters T_{eff} , $\log g$, $V \sin i$, and RV obtained by fitting the observed spectra, as well as the spectral classification deduced on one hand from $T_{\text{eff}}-\log g$ plane calibration (CFP determination, method 2) and on the other hand from equivalent width diagrams (CEW determination, method 1), are reported in columns 7, 8, 9 and 10, respectively. As the heliocentric velocities are smaller than 1.5 km s $^{-1}$ and the mean error on RV are 9-10 km s $^{-1}$, we do not correct RV from the heliocentric velocity.

4.1.2. Luminosity, mass, and radius for O-B-A stars

Once the fundamental parameters of O, B, and A stars are known, to derive their luminosity, mass and radius, we interpolate in the HR-diagram grids calculated for the LMC metal-

Table 3. Parameters for O-B-A stars that need no corrections for fast rotation. KWBBE names from Keller et al. (1999) or our MHF catalogue numbers are given in col. 1. Coordinates ($\alpha(2000)$, $\delta(2000)$) are given in col. 2 and 3. The instrumental V magnitude and instrumental (B-V) colour index are given in col. 4 and 5. The S/N ratio is given in col. 6. In col. 7, 8, 9 and 10, T_{eff} is given in K, $\log g$ in dex, $V \sin i$ and RV in km s^{-1} . ‘CFP’ is the spectral type and luminosity classification determined from fundamental parameters (method 2), whereas ‘CEW’ is the spectral type and luminosity classification determined from EW diagrams (method 1). In the last column some complementary indications on the spectrum are given: ‘He II’ when the line at 4200 Å is observed, ‘bin’ in case of suspected binary, ‘not Be’ for a Be star suspected by Keller et al. (1999) but not seen as a Be star in our study. The last column also gives the localization in clusters: cl0 for NGC 2004 (05h 30m 42s -67° 17' 11"), cl1 for KMHK 988 (05h 30m 36.5s -67° 11' 09"), cl2 for KMHK 971 (05h 29m 55s -67° 18' 37"), cl3 for KMHK 930 (05h 28m 13s -67° 07' 21"), cl4 for KMHK 943 (05h 28m 35s -67° 13' 29"), cl5 for the ‘unknown’ cluster or association 1 (05h 30m 25s -67° 13' 20"), cl6 for the ‘unknown’ cluster or association 2 (05h 29m 54s -67° 07' 37"), cl7 for the ‘unknown’ cluster or association 3 (05h 27m 21s -67° 12' 52"), cl8 for the association BSDL 1930 (05h 29m 26s -67° 08' 54"), and cl9 for the galactic open cluster HS 66325 (05h 29m 36s -67° 07' 41").

Star	α	δ	V	B-V	S/N	T_{eff}	$\log g$	$V \sin i$	RV	CFP	CEW	comm.
MHF52224	5 29 10.474	-67 24 33.16	15.22	0.18	95	22000 ±1300	3.5 ±0.2	11 ±20	311 ±10	B2III-IV	B1.5III	
MHF54275	5 27 43.510	-67 23 57.52	16.46	0.19	90	23500 ±1400	4.1 ±0.2	37 ±20	309 ±10	B1V	B2IV	
MHF54565	5 27 59.431	-67 24 08.32	14.76	0.19	120	24000 ±1200	3.6 ±0.2	172 ±10	318 ±10	B1IV	B0V	
MHF54686	5 27 50.434	-67 23 57.74	16.21	0.27	80	20000 ±1200	4.0 ±0.2	210 ±20	300 ±10	B2V	B3V	
MHF57079	5 28 08.580	-67 23 28.10	16.39	0.25	50	24000 ±2900	4.2 ±0.4	320 ±50	295 ±10	B1V	B2.5V	
MHF57428	5 28 10.900	-67 23 21.10	16.28	0.20	70	25000 ±2000	4.3 ±0.3	53 ±10	307 ±10	B1V	B1V	
MHF57975	5 30 13.775	-67 23 21.25	16.42	0.18	70	20000 ±1600	3.8 ±0.3	345 ±35	301 ±10	B2IV	B1.5V	
MHF59059	5 27 40.443	-67 23 00.64	15.65	0.18	90	24500 ±1500	4.3 ±0.3	71 ±10	317 ±10	B1V	B2V	
MHF60436	5 28 04.640	-67 22 49.20	16.44	0.18	75	23000 ±1800	4.1 ±0.3	165 ±17	305 ±10	B1.5V	B1.5V	
MHF62150	5 28 42.846	-67 22 22.93	16.47	0.18	70	18500 ±1500	4.0 ±0.3	40 ±20	304 ±10	B2V	B2V	
MHF62555	5 27 35.078	-67 22 17.96	16.08	0.18	85	20500 ±1600	4.0 ±0.3	84 ±10	304 ±10	B2V	B2V	
MHF63084	5 30 37.190	-67 22 14.70	15.97	0.19	50	10500 ±1200	2.9 ±0.3	26 ±20	292 ±10	B9.5III	B6.5IV	
MHF63948	5 28 19.782	-67 21 59.99	15.96	0.17	60	20500 ±2100	4.0 ±0.4	149 ±24	313 ±10	B2V	B2V	
MHF65925	5 27 40.477	-67 21 32.86	16.10	0.18	100	23000 ±1200	4.0 ±0.2	109 ±10	322 ±10	B1.5V	B1V	
MHF66708	5 28 58.020	-67 21 30.57	16.31	0.17	110	26500 ±1300	4.3 ±0.2	123 ±10	325 ±10	B1V	B1.5IV	
MHF67663	5 29 01.263	-67 21 19.99	15.63	0.20	120	30000 ±1500	4.3 ±0.2	9 ±20	306 ±10	B0V	B1IV	HeII
MHF67792	5 28 26.590	-67 21 12.50	16.44	0.17	80	22500 ±1400	4.0 ±0.2	57 ±10	300 ±10	B1.5V	B1.5V	
MHF68153	5 30 33.960	-67 21 17.30	16.13	0.18	60	22000 ±2200	4.0 ±0.4	186 ±30	300 ±10	B1.5V	B1.5IV	
MHF68195	5 27 39.477	-67 21 05.57	16.13	0.17	114	23000 ±1200	4.0 ±0.2	95 ±10	308 ±10	B1.5V	B1.5III	
MHF68257	5 29 30.810	-67 21 22.00	16.17	0.19	70	23000 ±1800	4.0 ±0.3	50 ±10	312 ±10	B1.5V	B1III	
MHF69681	5 28 33.460	-67 20 57.00	14.91	0.20	130	27000 ±1300	3.8 ±0.2	19 ±20	308 ±10	B1IV	B0V	
MHF70976	5 29 01.686	-67 20 39.36	15.64	0.19	110	32500 ±1600	4.3 ±0.2	30 ±20	326 ±10	B0V	B0V	HeII
MHF72268	5 29 46.090	-67 20 22.60	16.06	0.16	100	20000 ±1000	3.8 ±0.2	168 ±10	266 ±10	B2IV	B1.5III	
MHF74015	5 30 03.900	-67 20 01.50	16.39	0.16	70	22500 ±1800	4.1 ±0.3	118 ±12	300 ±10	B1.5V	B1.5V	
MHF75373	5 30 14.180	-67 19 43.90	16.49	0.16	65	20000 ±2000	4.0 ±0.4	104 ±14	299 ±10	B2V	B2III	
MHF75553	5 29 15.980	-67 19 45.65	15.16	0.17	140	19600 ±1000	3.6 ±0.2	33 ±20	315 ±10	B2IV	B1III	
MHF77981	5 29 28.020	-67 19 16.80	16.02	0.19	90	23000 ±1400	4.0 ±0.2	42 ±20	296 ±10	B1.5V	B1III	
MHF78706	5 30 06.370	-67 19 06.00	16.11	0.19	80	23000 ±1400	4.0 ±0.2	152 ±15	300 ±10	B1V	B1V	
MHF81136	5 30 29.230	-67 18 35.20	15.97	0.17	90	21000 ±1300	4.0 ±0.2	74 ±10	300 ±10	B2V	B2V	
MHF81174	5 28 55.258	-67 18 32.63	16.30	0.16	80	22000 ±1300	4.3 ±0.3	97 ±10	317 ±10	B1.5V	B2IV	
MHF81322	5 28 00.860	-67 18 32.84	15.24	0.19	85	29000 ±1700	4.5 ±0.3	183 ±15	319 ±10	B0V	B0.5V	HeII
MHF81490	5 29 56.010	-67 18 35.70	16.43	0.60	70	18000 ±1500	4.1 ±0.3	153 ±15	313 ±10	B2.5V	B2.5V	cl2
MHF81521	5 29 14.560	-67 18 33.70	15.15	0.18	90	17000 ±1000	3.5 ±0.2	69 ±10	293 ±10	B3III-IV	B2.5III	
MHF81807	5 29 45.660	-67 18 32.90	16.16	0.17	80	20000 ±1200	3.8 ±0.2	80 ±10	290 ±10	B2IV	B1.5V	
MHF82482	5 29 55.425	-67 18 27.88	16.27	0.45	80	22000 ±1300	4.0 ±0.2	50 ±10	318 ±10	B1.5V	B2V	cl2
MHF84042	5 29 31.731	-67 18 02.40	16.38	0.18	100	20500 ±1000	4.1 ±0.2	194 ±10	282 ±10	B2V	B2V	
MHF84176	5 28 01.745	-67 17 54.83	16.46	0.20	75	27000 ±2200	4.3 ±0.3	102 ±10	321 ±10	B1V	B1IV	
MHF85562	5 30 33.800	-67 17 44.90	16.13	0.17	65	20000 ±2000	4.0 ±0.4	71 ±12	305 ±10	B2V	B2V	cl0
MHF86995	5 29 26.755	-67 17 33.49	15.92	0.34	105	18500 ±900	3.7 ±0.2	11 ±20	297 ±10	B2.5IV	B2IV	
MHF87634	5 30 27.780	-67 17 22.50	15.27	0.18	148	26000 ±1300	3.9 ±0.2	234 ±12	310 ±10	B1V	B1III	cl0
MHF88527	5 28 21.190	-67 17 06.20	16.47	0.19	100	25000 ±1300	4.3 ±0.2	16 ±20	312 ±10	B1V	B1.5III	
MHF93347	5 29 46.957	-67 16 14.79	16.39	0.18	102	24000 ±1200	4.2 ±0.2	191 ±10	313 ±10	B1V	B1.5IV	
MHF94228	5 29 51.414	-67 16 03.90	16.38	0.18	90	19500 ±1200	3.9 ±0.2	127 ±10	337 ±10	B2V	B2III	
MHF95555	5 30 14.008	-67 15 52.75	16.28	0.19	85	19500 ±1200	3.7 ±0.2	320 ±30	299 ±10	B2IV	B1.5III	
MHF96072	5 27 09.328	-67 15 31.37	16.37	0.16	70	23000 ±1800	4.5 ±0.4	191 ±20	302 ±10	B1.5V	B2.5V	
MHF97219	5 27 47.076	-67 15 29.13	15.10	0.21	170	36000 ±1800	4.4 ±0.2	31 ±20	293 ±10	O8V	O5V	HeII+bin?
MHF97965	5 28 24.323	-67 15 20.11	16.33	0.15	95	21000 ±1300	4.3 ±0.3	131 ±10	300 ±10	B1.5V	B2.5V	

Table 3. continue

MHF98622	5 27 24.867	-67 15 05.31	15.99	0.17	120	19000 ±900	3.8 ±0.2	21 ±20	298 ±10	B3IV	B2IV	
MHF98629	5 30 01.360	-67 15 10.60	16.50	0.17	70	21000 ±1700	3.8 ±0.3	340 ±35	315 ±10	B2IV	B1III	
MHF100069	5 27 29.545	-67 14 52.44	16.18	0.27	95	19000 ±1100	4.1 ±0.2	204 ±15	301 ±10	B2V	B2.5V	
MHF101934	5 29 17.200	-67 14 40.60	15.99	0.17	90	15000 ±900	3.4 ±0.2	72 ±10	285 ±10	B5III-IV	B2.5III	
MHF105436	5 29 20.133	-67 13 55.71	15.64	0.17	116	19500 ±1000	3.6 ±0.2	134 ±10	292 ±10	B2III-IV	B2.5V	
MHF106600	5 30 47.920	-67 13 42.60	16.18	0.15	80	20500 ±1200	4.1 ±0.2	227 ±22	291 ±10	B2V	B2IV	
MHF106613	5 28 35.209	-67 13 45.45	16.31	0.33	91	17500 ±1100	3.6 ±0.2	324 ±25	300 ±10	B3III-IV	B2.5V	cl4
MHF106692	5 29 58.573	-67 13 47.01	14.89	0.18	145	15000 ±700	3.1 ±0.1	33 ±20	295 ±10	B5III	B5	
MHF107300	5 29 19.200	-67 13 34.20	16.07	0.17	70	25000 ±2000	4.0 ±0.3	24 ±20	292 ±10	B1IV-V	B1V	
MHF107458	5 30 36.450	-67 13 33.70	16.27	0.17	70	19500 ±1600	3.7 ±0.3	343 ±35	312 ±10	B2III-IV	B1III	
MHF109280	5 29 26.489	-67 13 12.50	16.43	0.17	125	19300 ±1000	3.8 ±0.2	57 ±10	270 ±10	B2IV-V	B2V	
MHF110170	5 29 18.147	-67 13 00.25	16.32	0.26	110	20500 ±1000	4.0 ±0.2	137 ±10	298 ±10	B2IV-V	B2IV	
MHF112935	5 27 31.570	-67 12 30.60	15.29	0.19	130	29000 ±1500	4.2 ±0.2	178 ±10	306 ±10	B0.5V	B0.5V	HeII
MHF113982	5 28 25.150	-67 12 17.33	16.00	0.17	108	21500 ±1100	3.8 ±0.2	51 ±10	301 ±10	B2IV	B1.5IV	
MHF115761	5 30 32.530	-67 12 00.40	16.12	0.16	74	23000 ±1900	4.0 ±0.3	23 ±20	307 ±10	B1.5V	B1V	
MHF115844	5 28 24.445	-67 12 00.22	16.34	0.17	100	18500 ±1000	3.9 ±0.2	103 ±10	294 ±10	B2.5IV	B2.5V	
MHF116094	5 27 10.510	-67 11 47.70	16.28	0.17	67	21000 ±2100	3.8 ±0.3	374 ±60	300 ±10	B2IV	B2V	
MHF117096	5 28 38.272	-67 11 41.86	16.26	0.18	70	20000 ±1600	3.9 ±0.3	19 ±20	305 ±10	B2V	B1V	
MHF117930	5 27 29.079	-67 11 29.27	16.29	0.16	80	26000 ±1600	4.4 ±0.3	191 ±20	373 ±10	B1V	B1.5V	
MHF117946	5 27 34.980	-67 11 28.60	16.32	0.16	85	20000 ±1200	4.1 ±0.2	129 ±13	299 ±10	B2V	B2V	
MHF119603	5 29 31.746	-67 11 17.65	15.61	0.16	118	21500 ±1100	3.9 ±0.2	49 ±15	300 ±10	B2V	B1.5V	
MHF119707	5 30 32.940	-67 11 22.20	15.15	0.18	120	21500 ±1100	3.6 ±0.2	134 ±10	308 ±10	B2III-IV	B1IV	cl1
MHF120461	5 30 36.730	-67 11 02.90	16.16	0.15	60	21000 ±2100	4.0 ±0.4	131 ±21	297 ±10	B2V	B1.5III	cl1
MHF121339	5 27 28.317	-67 10 53.78	14.95	0.18	120	25000 ±1200	3.9 ±0.2	19 ±20	300 ±10	B1V	B1V	
MHF122794	5 30 49.220	-67 10 43.70	16.30	0.20	50	22000 ±2600	4.0 ±0.4	53 ±20	298 ±10	B2V	B1V	
MHF124760	5 30 12.170	-67 10 19.50	15.28	0.17	110	24500 ±1200	3.8 ±0.2	172 ±10	329 ±10	B1V	B0V	
MHF124844	5 27 04.836	-67 10 05.99	16.23	0.20	85	16000 ±1000	3.5 ±0.2	166 ±15	300 ±10	B3III-IV	B2.5III	
MHF125614	5 30 17.430	-67 10 07.90	16.38	0.20	60	20500 ±2100	3.9 ±0.4	157 ±25	287 ±10	B2V	B1.5IV	
MHF126078	5 29 43.232	-67 10 00.82	16.02	0.18	86	21000 ±1300	3.8 ±0.2	38 ±20	312 ±10	B2IV	B1.5V	
MHF128212	5 29 53.238	-67 9 42.49	14.93	0.19	160	21000 ±1000	3.8 ±0.2	64 ±10	322 ±10	B2IV	B1.5V	
MHF131188	5 29 37.665	-67 9 05.80	15.24	0.18	140	30000 ±1500	4.3 ±0.2	325 ±16	299 ±10	B0V	B0.5V	HeII
MHF131563	5 30 31.970	-67 8 58.80	16.46	0.26	55	17500 ±1900	4.2 ±0.4	140 ±22	318 ±10	B3V	B3V	
MHF131570	5 29 51.860	-67 8 57.40	16.41	0.16	70	19500 ±1600	4.0 ±0.3	122 ±12	298 ±10	B2V	B2.5V	
MHF132507	5 28 18.853	-67 8 43.75	16.41	0.18	80	19500 ±1200	4.0 ±0.2	13 ±20	286 ±10	B2V	B2V	
MHF133049	5 29 52.694	-67 8 42.79	16.10	0.21	70	21000 ±1700	4.0 ±0.3	35 ±20	287 ±10	B2V	B1.5V	
MHF134545	5 30 14.008	-67 8 23.97	16.31	0.18	80	20000 ±1200	3.9 ±0.2	78 ±10	319 ±10	B2V	B2V	
MHF134864	5 29 18.600	-67 8 22.35	16.37	0.17	85	18000 ±1100	3.7 ±0.2	3 ±20	313 ±10	B2.5IV	B2.5IV	
MHF135232	5 28 38.670	-67 8 14.50	16.01	0.16	95	24500 ±1500	4.1 ±0.2	222 ±16	352 ±10	B1V	B1V	
MHF136076	5 28 47.904	-67 8 02.56	16.44	0.27	70	22000 ±1800	4.1 ±0.3	23 ±20	307 ±10	B2V	B2V	
MHF136846	5 30 03.662	-67 7 58.97	16.19	0.17	80	19500 ±1200	3.6 ±0.2	248 ±25	300 ±10	B2III-IV	B1V	
MHF136943	5 30 37.390	-67 7 56.00	16.24	0.23	60	19500 ±2000	4.1 ±0.4	205 ±33	299 ±10	B2V	B2III	
MHF137534	5 30 25.610	-67 7 50.70	16.17	0.19	63	21000 ±2100	3.9 ±0.4	107 ±17	313 ±10	B2V	B1V	
MHF137890	5 29 58.370	-67 7 44.37	16.32	0.17	85	21000 ±1300	4.1 ±0.2	123 ±11	295 ±10	B2V	B1V	cl6
MHF138223	5 29 36.708	-67 7 40.89	16.24	0.69	65	14500 ±1500	4.1 ±0.4	83 ±14	281 ±10	B5V	B6V	cl9
MHF139231	5 30 19.580	-67 7 34.20	14.92	0.18	75	21000 ±1700	3.6 ±0.3	168 ±17	297 ±10	B2III	B0.5IV	
MHF140653	5 30 21.138	-67 7 17.83	15.21	0.19	75	20500 ±1600	3.9 ±0.3	52 ±20	272 ±10	B2IV	B2IV	
MHF141004	5 29 57.130	-67 7 35.50	15.14	0.33	115	32500 ±1600	4.4 ±0.2	21 ±20	296 ±10	O9V	O9V	HeII, cl6
MHF141834	5 28 17.049	-67 6 54.57	16.38	0.16	90	22500 ±1300	4.0 ±0.2	129 ±10	311 ±10	B2V	B2IV	cl3
MHF142249	5 28 13.500	-67 6 54.80	16.46	0.21	80	18500 ±1100	3.9 ±0.2	87 ±10	312 ±10	B2.5V	B2.5IV	cl3
MHF142489	5 29 35.870	-67 6 51.20	16.35	0.16	50	9600 ±1200	3.2 ±0.3	1 ±20	288 ±10	A0.5III	B9III	
MHF142798	5 29 41.935	-67 6 47.67	16.47	0.17	70	19500 ±1600	4.1 ±0.3	149 ±15	303 ±10	B2V	B2.5V	
MHF144083	5 30 07.760	-67 6 34.71	16.27	0.19	80	22000 ±1300	4.0 ±0.2	241 ±25	300 ±10	B2V	B1V	
MHF144186	5 30 19.070	-67 6 36.00	16.05	0.19	63	19000 ±1900	3.7 ±0.3	169 ±30	290 ±10	B2III-IV	B1III	
MHF144562	5 28 19.926	-67 6 24.61	16.40	0.16	90	13500 ±800	3.6 ±0.2	167 ±12	299 ±10	B5III	B3III	
MHF144608	5 30 37.355	-67 6 29.83	15.64	0.19	100	21000 ±1100	3.7 ±0.2	18 ±20	309 ±10	B2IV	B1V	
MHF144637	5 30 32.420	-67 6 32.40	14.96	0.18	85	21000 ±1300	3.5 ±0.2	202 ±20	248 ±10	B2III-IV	B1IV	
KWBBe0554	5 30 19.794	-67 17 05.02	16.74	0.30	56	18500 ±2200	4.2 ±0.4	47 ±20	310 ±10	B2.5V	B2.5V	not Be
KWBBe0993	5 30 18.581	-67 18 51.61	17.38	0.16	60	19500 ±2000	4.2 ±0.4	33 ±20	307 ±10	B2V	B2.5V	not Be
KWBBe1169	5 30 45.160	-67 17 18.30	16.62	1.33	40	15500 ±2300	4.1 ±0.4	283 ±57	300 ±10	B4V	B6III	not Be, cl0

Table 5. Corrections for $\Omega/\Omega_c = 85\%$ for rapidly rotating B stars in the sample. The units are K for T_{eff}^o , dex for $\log g_o$, and km s^{-1} for $V\sin i^{\text{true}}$.

Star	Ω/Ω_c	$= 85\%$	
	T_{eff}^o	$\log g_o$	$V\sin i^{\text{true}}$
MHF57079	25000±2900	4.4±0.4	327±50
MHF57975	21500±1600	4.1±0.3	357±35
MHF95555	21000±1200	4.0±0.2	331±30
MHF98629	22500±1700	4.1±0.3	348±35
MHF106613	19500±1100	4.0±0.2	338±25
MHF107458	22000±1600	4.0±0.3	350±35
MHF116094	23000±2100	4.1±0.3	384±60
MHF131188	31000±1500	4.4±0.2	333±16
KWBBel169	16500±2400	4.4±0.4	294±57

licity ($Z = 0.004$; Korn et al. 2002, Rolleston et al. 1996) and for stars without rotation in Charbonnel et al. (1993).

In order to justify the use of non-rotating models, we estimate the mean radius, mean mass and mean $V\sin i$ in various mass bins (e.g. $5 < M < 7 M_\odot$, $7 < M < 9 M_\odot$, etc). We then obtain a mean equatorial velocity for a random angle distribution using:

$$V_e = \frac{4}{\pi} \langle V\sin i_{\text{app.}} \rangle, \quad (1)$$

where $\langle V\sin i_{\text{app.}} \rangle$ is the mean $V\sin i_{\text{app.}}$.

We calculate the critical velocity with the classical formula:

$$V_c \simeq 436.7 \left(\frac{\langle M \rangle}{\langle R \rangle} \right)^{1/2}, \quad (2)$$

where $\langle M \rangle$ and $\langle R \rangle$ are the mean mass in M_\odot and mean radius in R_\odot .

This gives the V_e/V_c ratio, and we can then obtain Ω/Ω_c thanks to formulae taken from Chauville et al. (2001):

$$\Omega/\Omega_c = \frac{1}{0.724} V_e/V_c [1 - 0.276(V_e/V_c)^2]. \quad (3)$$

For B stars $\langle V\sin i_{\text{app.}} \rangle$ is close to 110 km s^{-1} , thus $V_e/V_c \simeq 27\%$ and $\Omega/\Omega_c \simeq 37\%$. As the effects of fast rotation appear for $\Omega/\Omega_c > 50\%$ (Zorec et al. 2005), we do not need to correct B stars for fast rotation effects except for 9 of them which have a strong $V\sin i$.

We obtain in this way the luminosity, mass and radius of most O, B and A stars of the sample (see Table 4). The position of these stars in the HR diagram is shown in Fig. 5.

4.2. Corrections for rapidly rotating B-type stars

The 9 B-type stars MHF57079, MHF57975, MHF95555, MHF98629, MHF106613, MHF107458, MHF116094, MHF131188, and KWBBel169 have a high rotational velocity, although they do not show emission lines as Be stars. The star KWBBel169 was previously observed like a Be star by Keller (1999) but, in our observations, it does not show any emission. This could be due to the transient nature of the Be phenomenon. Results on fundamental parameters taking into account fast rotation effects are given in Table 5 and Fig. 5.

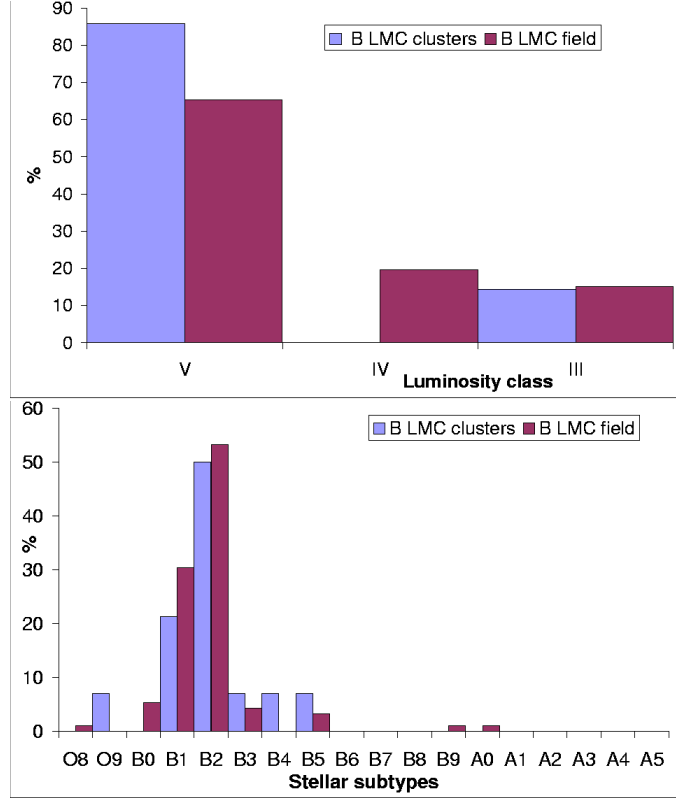


Fig. 6. Luminosity class (upper panel) and spectral type (lower panel) distributions of B-type stars in the sample in the LMC.

4.3. Be stars

4.3.1. Fundamental parameters of Be stars

The total number of Be stars in the sample is 47. It includes 22 known Be stars, called KWBBel in Keller et al. (1999), for which the $H\alpha$ emissive character has been confirmed, and 25 new Be stars reported in Paper I and called MHFBe. For a description of the emission line characteristics of these stars we refer to Paper I. The apparent fundamental parameters ($T_{\text{eff}}^{\text{app.}}$, $\log g_{\text{app.}}$, $V\sin i_{\text{app.}}$, and RV) we derive in a first step for these stars are reported in Table 7. The spectral classification derived from apparent fundamental parameters is also given in the last column of the Table. Without correction for fast rotation nearly all Be stars would have a sub-giant or giant luminosity class. The apparent position of Be stars in the HR diagram compared to B stars is also shown in Fig. 5.

4.3.2. Rapid rotation corrections for Be stars

The pncr (i.e. parent non rotating counterpart) fundamental parameters (T_{eff}^o , $\log g_o$, $V\sin i^{\text{true}}$) we obtain after correction with FASTROT (see Sect. 3.4) are given in Table 8 for different rotation rates Ω/Ω_c . We estimate the rotation rate Ω/Ω_c to be used for the selection of the probable most suitable pncr fundamental parameters of Be stars in the LMC thanks to the equations mentioned above. We obtain $V_e/V_c \simeq 70\%$ and $\Omega/\Omega_c \simeq 85\%$ on average. As for O-B-A stars and with the pncr fundamental parameters corresponding to the rotation rate $\Omega/\Omega_c = 85\%$, we

Table 4. Parameters $\log(L/L_{\odot})$, M/M_{\odot} and R/R_{\odot} interpolated or calculated for our sample of O-B stars and for several SB1 from HR diagrams taken from Charbonnel et al. (1993).

Star	$\log(L/L_{\odot})$	M/M_{\odot}	R/R_{\odot}	Star	$\log(L/L_{\odot})$	M/M_{\odot}	R/R_{\odot}
MHF52224	4.2±0.3	10.0±1.0	9.2±1.0	MHF107300	4.0±0.3	9.7±0.5	5.3±1.0
MHF54275	3.7±0.3	8.4±0.5	4.5±0.5	MHF107458	3.8±0.3	7.4±0.5	6.8±1.0
MHF54565	4.4±0.3	11.3±1.0	9.1±1.0	SBMHF109251	3.5±0.3	6.9±0.5	4.7±0.5
MHF54686	3.3±0.3	6.1±0.5	3.9±0.5	MHF109280	3.5±0.3	6.5±0.5	5.4±1.0
MHF57079	3.6±0.3	8.1±0.5	3.6±0.5	MHF110170	3.5±0.3	6.7±0.5	4.3±0.5
MHF57428	3.6±0.3	8.4±0.5	3.2±0.5	SBMHF110467	3.9±0.3	10.1±1.0	4.5±0.5
MHF57975	3.7±0.3	7.0±0.5	5.9±1.0	MHF112935	4.1±0.3	12.0±1.0	4.6±0.5
MHF59059	3.5±0.3	8.2±0.5	3.2±0.5	SBMHF113048	3.4±0.3	5.8±0.5	5.5±1.0
MHF60436	3.7±0.3	8.0±0.5	4.6±0.5	MHF113982	3.8±0.3	8.2±0.5	5.8±1.0
MHF62150	3.2±0.3	5.8±0.5	4.1±0.5	MHF115761	3.8±0.3	8.5±0.5	5.1±1.0
MHF62555	3.5±0.3	6.7±0.5	4.2±0.5	MHF115844	3.4±0.3	6.1±0.5	4.9±0.5
MHF63084	3.3±0.3	5.2±0.5	14.3±1.5	MHF116094	3.8±0.3	8.0±0.5	5.8±1.0
MHF63948	3.4±0.3	6.6±0.5	4.1±0.5	MHF117096	3.5±0.3	6.8±0.5	4.8±0.5
MHF65925	3.8±0.3	8.5±0.5	4.9±0.5	MHF117930	3.6±0.3	8.2±0.5	3.0±0.5
MHF66708	3.8±0.3	9.6±0.5	3.7±0.5	MHF117946	3.4±0.3	6.4±0.5	3.9±0.5
MHF67663	4.1±0.3	12.5±1.0	4.3±0.5	MHF119603	3.6±0.3	7.6±0.5	4.9±0.5
MHF67792	3.7±0.3	8.0±0.5	4.7±0.5	MHF119707	4.1±0.3	9.0±0.5	8.2±1.0
MHF68153	3.7±0.3	7.8±0.5	4.6±0.5	MHF120461	3.5±0.3	6.9±0.5	4.2±0.5
MHF68195	3.8±0.3	8.4±0.5	4.7±0.5	MHF121339	4.1±0.3	10.4±1.0	6.0±1.0
MHF68257	3.7±0.3	8.1±0.5	4.6±0.5	MHF122794	3.6±0.3	7.6±0.5	4.7±0.5
MHF69681	4.4±0.3	12.9±1.0	7.3±1.0	MHF124760	4.1±0.3	10.7±1.0	6.7±1.0
MHF70976	4.3±0.3	15.0±1.0	4.8±0.5	MHF124844	3.5±0.3	6.1±0.5	7.4±1.0
MHF72268	3.6±0.3	7.2±0.5	5.6±1.0	MHF125614	3.6±0.3	7.0±0.5	4.8±0.5
MHF74015	3.6±0.3	7.9±0.5	4.4±0.5	MHF126078	3.8±0.3	8.3±0.5	6.1±1.0
MHF75373	3.4±0.3	6.6±0.5	4.2±0.5	MHF128212	3.7±0.3	7.8±0.5	5.7±1.0
MHF75553	3.9±0.3	8.1±0.5	8.1±1.0	SBMHF128963	3.4±0.3	6.6±0.5	4.2±0.5
MHF77981	3.7±0.3	8.2±0.5	4.7±0.5	MHF131188	4.1±0.3	12.4±1.0	4.0±0.5
MHF78706	3.7±0.3	8.3±0.5	4.6±0.5	MHF131563	2.8±0.2	4.5±0.5	2.8±0.5
MHF81807	3.6±0.3	7.2±0.5	5.6±0.5	MHF131570	3.3±0.3	6.1±0.5	4.0±0.5
MHF81136	3.5±0.3	6.9±0.5	4.4±0.5	MHF132507	3.4±0.3	6.4±0.5	4.4±0.5
MHF81174	3.3±0.3	6.7±0.5	3.1±0.5	MHF133049	3.5±0.3	7.0±0.5	4.4±0.5
MHF81322	3.7±0.3	7.0±0.5	2.7±0.5	MHF134545	3.5±0.3	6.7±0.5	4.6±0.5
MHF81490	3.1±0.3	5.2±0.5	3.4±0.5	MHF134864	3.5±0.3	6.3±0.5	5.9±1.0
MHF81521	3.6±0.3	6.6±0.5	7.8±1.0	MHF135232	3.8±0.3	9.1±0.5	4.6±0.5
MHF82482	3.6±0.3	7.4±0.5	4.4±0.5	MHF136076	3.6±0.3	7.4±0.5	4.1±0.5
MHF84042	3.3±0.3	6.4±0.5	3.6±0.5	MHF136846	3.8±0.3	7.3±0.5	7.0±1.0
MHF84176	3.8±0.3	10.1±1.0	3.7±0.5	MHF136943	3.3±0.3	6.2±0.5	3.9±0.5
MHF85562	3.4±0.3	6.5±0.5	4.2±0.5	MHF137534	3.6±0.3	7.4±0.5	5.0±0.5
MHF86995	3.5±0.3	6.5±0.5	6.0±1.0	MHF137890	3.5±0.3	6.9±0.5	4.1±0.5
MHF87634	4.1±0.3	11.1±1.0	5.9±1.0	MHF138223	2.5±0.2	3.6±0.5	2.7±0.5
MHF88527	3.7±0.3	8.5±0.5	3.3±0.5	MHF139231	4.0±0.3	8.8±0.5	8.3±1.0
MHF93347	3.6±0.3	8.1±0.5	3.8±0.5	MHF140653	3.6±0.3	7.1±0.5	5.0±0.5
MHF94228	3.4±0.3	6.6±0.5	4.6±0.5	MHF141004	4.1±0.3	8.9±0.5	3.2±0.5
MHF95555	3.7±0.3	7.1±0.5	6.4±1.0	MHF141834	3.7±0.3	7.8±0.5	4.5±0.5
MHF96072	3.1±0.3	4.8±0.5	2.2±0.5	SBMHF141891	3.5±0.3	6.8±0.5	4.5±0.5
MHF97219	4.4±0.3	11.9±1.0	3.8±0.5	MHF142249	3.3±0.3	6.0±0.5	4.5±0.5
MHF97965	3.2±0.3	6.2±0.5	2.9±0.5	MHF142489	2.6±0.2	3.4±0.5	7.6±1.0
MHF98622	3.5±0.3	6.5±0.5	5.6±1.0	MHF142798	3.2±0.3	5.9±0.5	3.4±0.5
MHF98629	3.8±0.3	8.0±0.5	6.0±1.0	MHF144083	3.6±0.3	7.6±0.5	4.3±0.5
MHF100069	3.1±0.3	5.6±0.5	3.6±0.5	MHF144186	3.7±0.3	7.1±0.5	6.7±1.0
MHF101934	3.3±0.3	5.4±0.5	7.4±1.0	MHF144562	3.0±0.3	4.3±0.5	5.7±1.0
SBMHF102053	3.3±0.3	5.5±0.5	5.6±1.0	MHF144608	3.9±0.3	8.2±0.5	6.5±1.0
SBMHF103207	4.0±0.3	9.8±0.5	6.4±1.0	MHF144637	4.2±0.3	10.0±0.5	10.2±1.0
MHF105436	3.9±0.3	8.0±0.5	8.1±1.0	KWBBE0554	3.0±0.3	5.2±0.5	3.2±0.5
MHF106600	3.4±0.3	6.6±0.5	4.0±0.5	KWBBE0993	3.0±0.3	5.5±0.5	2.9±0.5
MHF106613	3.6±0.3	6.6±0.5	7.2±1.0	KWBBE1169	2.7±0.2	4.0±0.5	2.9±0.5
MHF106692	3.8±0.3	7.5±0.5	13.3±1.5				

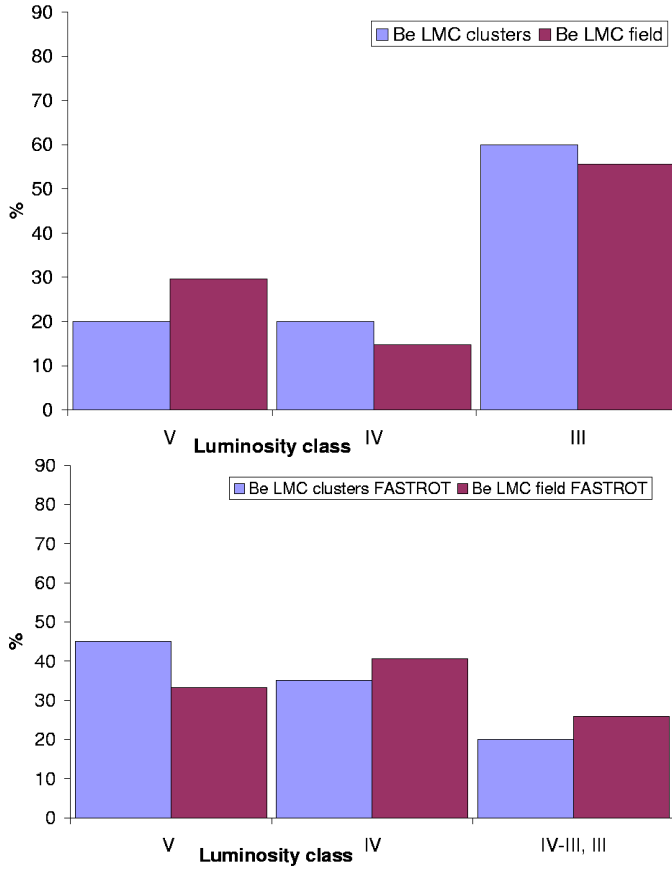


Fig. 7. Percentages of Be stars in the sample in the field and in clusters in the LMC versus luminosity class. Upper panel: without correction for fast rotation. Lower panel: with FASTROT corrections.

derive $\log(L/L_{\odot})$, M/M_{\odot} , and R/R_{\odot} for Be stars. These parameters are given in Table 9. After correction for rapid rotation, Be stars globally shift in the HR diagram towards lower luminosity and higher temperature, as illustrated in Fig. 5. It clearly demonstrates that Be stars are less evolved than their apparent fundamental parameters could indicate.

4.4. Spectroscopic binaries

The determination of fundamental parameters was undertaken for 15 spectroscopic binaries that show a single line spectrum (SB1, see Table 2 in Paper I). However, since we usually obtained only one spectrum for each suspected SB1 binary, the influence of the secondary component on the spectrum is not known. Results are given in Table 6. We note a fair agreement between spectral classifications derived from fundamental parameters and from the equivalent width of the $H\gamma$ and He I 4471 lines, except for one star (MHF91603). The mean $V \sin i$ for these binaries is 100 km s^{-1} .

4.5. Characteristics of the sample

To characterize the sample of stars, we study the distribution in spectral types, luminosity classes and masses for stars in clus-

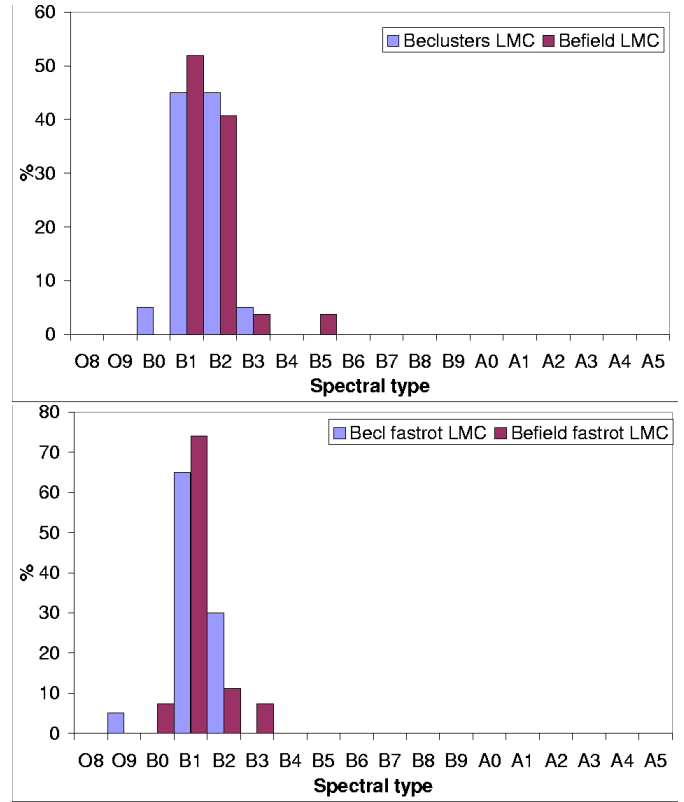


Fig. 8. Same as in Fig. 7, versus spectral type.

ters and in the field. These results are presented in the following subsections.

4.5.1. O-B-A stars

We present in Fig. 6 the distribution of O-B-A stars with respect to spectral type and luminosity class. The classification used here is the one obtained from the fundamental parameters determination.

Fig. 6 indicates that the B stars in the sample are essentially early B-type stars (B0 to B3) and are mainly dwarfs (class V), in the field as well as in clusters.

4.5.2. Be stars

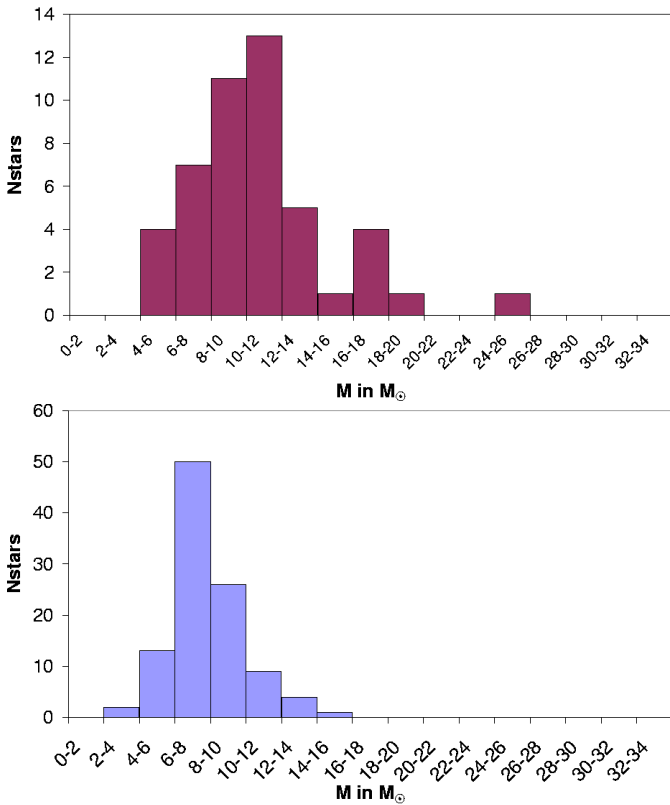
As in Sect. 4.5.1, we present the distribution of Be stars with respect to luminosity class and spectral type. Again the classification used here is the one obtained from the fundamental parameters determination. We also compare the distribution obtained before and after correction of fast rotation effects.

Fig. 7 shows that Be stars after fast rotation treatment appear less evolved than apparent parameters would suggest: some stars in classes III and IV are redistributed in classes IV and V, but about 60% of the Be stars still appear as giants and subgiants.

Fig. 8 presents the distribution in spectral types for Be stars before and after fast rotation treatment. The stars corrected for rotation effects appear hotter than apparent fundamental parameters would suggest. In particular there are more B1 types.

Table 6. Same as Table 3 for spectroscopic binaries.

Star	α (2000)	δ (2000)	V	B-V	S/N	T_{eff}	$\log g$	$V \sin i$	RV	CFP	CEW	comm.
MHF64847	5 27 32.040	-67 21 53.20	15.13	0.21	110	26000 \pm 1300	4.1 \pm 0.2	137 \pm 10	347 \pm 10	B1V	B1V	
MHF65587	5 28 23.460	-67 21 41.30	16.01	0.23	120	21500 \pm 1100	3.8 \pm 0.2	173 \pm 10	336 \pm 10	B1.5IV	B1V	
MHF71137	5 28 46.650	-67 20 40.90	15.62	0.24	107	21500 \pm 1100	4.0 \pm 0.2	117 \pm 10	321 \pm 10	B1.5V	B1.5IV	
MHF79301	5 29 11.050	-67 18 58.90	15.61	0.23	85	18000 \pm 1100	3.5 \pm 0.2	39 \pm 20	319 \pm 10	B2III-IV	B2III	
MHF91603	5 28 03.400	-67 16 33.20	15.19	0.24	140	19000 \pm 1000	3.5 \pm 0.2	54 \pm 10	322 \pm 10	B2III-IV	B1IV	
MHF98013	5 30 32.650	-67 15 25.70	14.82	0.25	120	19500 \pm 1000	3.5 \pm 0.2	89 \pm 10	277 \pm 10	B2III-IV	B0.5III	
MHF102053	5 29 56.242	-67 14 32.95	16.26	0.31	85	17000 \pm 1000	3.7 \pm 0.2	188 \pm 19	340 \pm 10	B3IV	B3V	
MHF103207	5 30 13.560	-67 14 27.10	14.94	0.23	140	23500 \pm 1200	3.8 \pm 0.2	122 \pm 10	221 \pm 10	B1IV	B1III	
MHF109251	5 28 31.950	-67 13 11.90	15.95	0.25	108	20500 \pm 1000	3.9 \pm 0.2	5 \pm 20	284 \pm 10	B2IV-V	B2IV	cl4
MHF110467	5 27 25.310	-67 12 52.50	15.70	0.17	123	26500 \pm 1300	4.1 \pm 0.2	31 \pm 20	264 \pm 10	B1V	B1V	cl7
MHF111340	05 27 14.43	-67 12 40.90	16.16	0.21	90					SB2	SB2	cl7
MHF113048	5 26 57.527	-67 12 18.95	16.38	0.21	90	17000 \pm 1000	3.7 \pm 0.2	75 \pm 10	283 \pm 10	B3IV	B2IV	
MHF128963	5 30 38.290	-67 9 32.70	15.95	0.25	75	20000 \pm 1600	4.0 \pm 0.3	97 \pm 10	314 \pm 10	B2V	B2.5V	
MHF133975	5 29 50.610	-67 8 30.00	16.27	0.25	80	21000 \pm 1300	4.0 \pm 0.2	79 \pm 10	233 \pm 10	B2V	B2IV	
MHF141891	5 28 00.770	-67 6 55.50	16.29	0.28	90	20500 \pm 1200	4.0 \pm 0.2	165 \pm 12	266 \pm 10	B2V	B2III	
MHF149652	5 28 58.672	-67 5 29.28	16.50	0.24	90	20000 \pm 1200	3.9 \pm 0.2	122 \pm 12	341 \pm 10	B2IV	B2IV	

**Fig. 9.** Mass distribution of Be (upper panel) and B stars (lower panel) in the sample in the LMC.

Nevertheless, in both distributions the sample is composed of early-type stars (B0 to B3).

4.5.3. Masses

In addition, we investigate the mass distribution of B and Be stars (Fig. 9). The sample shows a distribution peaking around 7 and 10 M_{\odot} for B and Be stars, respectively. Among the stars with $M \leq 9 M_{\odot}$ 18% are Be stars, whereas among the stars

with $M > 9 M_{\odot}$ 62% are Be stars. This is probably due to a bias effect in the target selection procedure, since the sample includes 61% of Be stars among stars brighter than $V=15$.

5. Rotational velocity and metallicity: results and discussion

In the following subsections, we first give some preliminary remarks about the study by Gies & Huang (2004) on B-type stars in clusters of the Milky Way (MW), which are used as a central thread in our study. Then we summarize results on $V \sin i$ we obtained for B and Be stars in the LMC. Finally, we compare these results with previous studies in the LMC and in the MW, and we discuss the effect of age and metallicity on rotational velocity.

5.1. Ages, $V \sin i$, and Be stars

Gies & Huang (2004, hereafter GH04) studied the link between rotational velocity and age in clusters of the MW. They noted a good agreement for the rotational velocity between data and predictions by Meynet & Maeder (2000) for a 12 M_{\odot} star and for clusters with $\log(t) \leq 7$. However, clusters with $\log(t) > 7$ seem to rotate faster than predicted. According to GH04, there could be several explanations: binarity, initial spin rates, and rotational velocity dependence on mass. For $\log(t) \leq 7$ the mean fraction of binaries calculated from the fraction given by GH04 for each cluster is $\frac{S_B}{all} = 15\%$, whereas for $\log(t) > 7$, $\frac{S_B}{all} = 19\%$. Therefore, binaries do not seem to be at the origin of the difference in rotational velocity.

As GH04 merged B and Be stars in their sample and as Be stars are fast rotators, a possible explanation of the differences in rotational velocity may be the proportion of Be stars in the clusters. We therefore searched in the WEBDA database¹ for the amount of Be stars in the clusters studied by GH04 and calculated the average percentages of Be stars for clusters younger

¹ The WEBDA database is maintained by J.C. Mermilliod. See <http://obswww.unige.ch/webda/navigation.html>

Table 7. Fundamental parameters of Be stars in the observed sample. Col. 1 gives the name of the star. Coordinates ($\alpha(2000)$, $\delta(2000)$) are given in col. 2 and 3. The instrumental V magnitude and instrumental (B-V) colour index are given in col. 4 and 5. The S/N ratio is given in col. 6. Col. from 7 to 10 give the apparent $T_{\text{eff}}^{\text{app}}$ in K, apparent $\log g_{\text{app}}$ in dex, apparent $V \sin i_{\text{app}}$ in km s^{-1} and RV in km s^{-1} . ‘CFP’ (col. 11) gives the spectral type and luminosity class derived from the fundamental parameters. The last column gives some complementary remarks about the localization in clusters: c10 for NGC 2004 (05h 30m 42s -67° 17' 11''), c11 for KMHK 988 (05h 30m 36.5s -67° 11' 09''), c12 for KMHK 971 (05h 29m 55s -67° 18' 37''), c13 for KMHK 930 (05h 28m 13s -67° 07' 21''), c14 for KMHK 943 (05h 28m 35s -67° 13' 29''), c15 for the ‘unknown’ cluster or association 1 (05h 30m 25s -67° 13' 20''), c16 for the ‘unknown’ cluster or association 2 (05h 29m 54s -67° 07' 37''), c17 for the ‘unknown’ cluster or association 3 (05h 27m 21s -67° 12' 52''), c18 for the association BSDL 1930 (05h 29m 26s -67° 08' 54'') and c19 for the galactic open cluster HS 66325 (05h 29m 36s -67° 07' 41'').

Star	$\alpha(2000)$	$\delta(2000)$	V	B-V	S/N	$T_{\text{eff}}^{\text{app}}$	$\log g_{\text{app}}$	$V \sin i_{\text{app}}$	RV	CFP	comm.
KWBBe0044	5 30 45.049	-67 14 26.14	13.70	0.24	140	23000 ±1100	3.2 ±0.2	111 ±10	319 ±10	B2III	
KWBBe0075	5 30 37.690	-67 17 39.50	14.41	0.43	90	23500 ±1400	3.5 ±0.2	185 ±13	312 ±10	B1III	c10
KWBBe0091	5 30 44.284	-67 17 22.72	14.44	0.33	140	20000 ±1000	3.2 ±0.2	201 ±10	301 ±10	B2III	c10
KWBBe0152	5 30 24.391	-67 14 55.50	15.58	0.18	103	23000 ±1200	3.4 ±0.2	379 ±19	300 ±10	B2III	
KWBBe0171	5 30 36.340	-67 16 51.00	15.55	0.30	110	23000 ±1100	3.6 ±0.2	270 ±14	290 ±10	B2III	c10
KWBBe0177	5 30 39.582	-67 16 49.63	15.27	0.39	83	30000 ±1800	3.5 ±0.2	491 ±50	301 ±10	B0III	c10
KWBBe0203	5 30 48.700	-67 16 49.30	15.35	0.42	80	24500 ±1500	3.3 ±0.2	256 ±25	301 ±10	B1III	c10
KWBBe0276	5 29 59.358	-67 14 46.49	15.79	0.22	119	22000 ±1100	3.3 ±0.2	246 ±12	273 ±10	B2III	
KWBBe0287	5 30 08.070	-67 14 36.20	15.83	0.17	90	20000 ±1200	3.2 ±0.2	221 ±15	275 ±10	B2III	
KWBBe0323	5 30 31.976	-67 16 40.26	16.21	0.17	90	23500 ±1400	3.7 ±0.2	274 ±19	302 ±10	B1.5III	c10
KWBBe0342	5 30 38.630	-67 16 23.00	16.04	0.19	80	23000 ±1400	4.1 ±0.2	309 ±31	323 ±10	B1.5V	c10
KWBBe0344	5 30 38.859	-67 14 21.13	15.89	0.18	100	22500 ±1100	3.8 ±0.2	216 ±11	301 ±10	B2IV	
KWBBe0347	5 30 39.900	-67 12 21.01	16.04	0.17	95	22500 ±1400	3.5 ±0.2	334 ±23	302 ±10	B2III	
KWBBe0374	5 30 47.799	-67 11 36.43	16.37	0.30	60	22000 ±2200	4.1 ±0.4	337 ±54	339 ±10	B2V	
KWBBe0579	5 30 27.610	-67 13 00.21	16.53	0.15	55	19000 ±2300	3.5 ±0.4	310 ±50	301 ±10	B2III	c15
KWBBe0622	5 30 36.223	-67 13 27.71	16.89	0.25	60	16000 ±1600	3.5 ±0.3	299 ±48	302 ±10	B3III	
KWBBe0624	5 30 37.400	-67 21 02.62	16.73	0.19	54	19670 ±2400	3.4 ±0.3	343 ±55	275 ±10	B2III	
KWBBe0874	5 29 55.846	-67 19 14.27	17.56	0.16	45	19000 ±2900	4.1 ±0.4	262 ±52	300 ±10	B2V	
KWBBe1055	5 30 29.265	-67 17 01.65	17.41	0.17	50	22000 ±2600	3.9 ±0.4	419 ±67	300 ±10	B2IV	c10
KWBBe1108	5 30 37.238	-67 11 29.31	17.64	0.20	50	19500 ±2300	4.0 ±0.4	316 ±51	300 ±10	B2V	c11
KWBBe1175	5 30 46.960	-67 17 39.30	17.75	0.12	25	21500 ±4300	4.2 ±0.4	345 ±100	297 ±10	B2V	c10
KWBBe1196	5 30 50.893	-67 18 08.51	17.56	0.16	45	17000 ±2200	3.8 ±0.4	359 ±65	299 ±10	B3IV	c10
MHFBBe55075	5 30 15.660	-67 23 54.60	16.01	0.26	50	21500 ±2600	3.8 ±0.4	266 ±43	301 ±10	B2IV	
MHFBBe55920	5 27 42.256	-67 23 36.58	16.08	0.16	80	23500 ±1400	4.0 ±0.2	120 ±12	304 ±10	B1V	
MHFBBe59721	5 29 25.670	-67 23 02.40	16.46	0.18	85	18000 ±1090	4.0 ±0.2	196 ±18	299 ±10	B2V	
MHFBBe66252	5 29 18.200	-67 21 37.10	16.26	0.17	80	25000 ±1500	4.0 ±0.2	446 ±45	274 ±10	B1V	
MHFBBe72704	5 28 29.430	-67 20 20.10	14.86	0.19	150	23000 ±1100	3.5 ±0.2	108 ±10	304 ±10	B1.5III-IV	
MHFBBe73013	5 28 55.994	-67 20 14.55	16.16	0.19	100	25000 ±120	4.3 ±0.2	402 ±20	302 ±10	B1V	
MHFBBe77796	5 29 13.609	-67 19 18.70	14.91	0.18	90	25500 ±1500	3.7 ±0.2	120 ±10	311 ±10	B1III-IV	
MHFBBe85028	5 29 45.000	-67 17 50.50	16.07	0.17	100	23000 ±1200	3.8 ±0.2	269 ±13	316 ±10	B1.5IV	
MHFBBe101350	5 30 34.640	-67 14 45.30	15.30	0.19	120	24500 ±1200	3.8 ±0.2	224 ±11	285 ±10	B1IV	
MHFBBe103914	5 27 15.216	-67 14 10.15	15.03	0.17	130	26500 ±1300	3.4 ±0.2	368 ±18	300 ±10	B1III	
MHFBBe107771	5 28 34.651	-67 13 23.97	16.39	0.37	84	18000 ±1100	3.6 ±0.2	319 ±29	300 ±10	B2.5III-IV	c14
MHFBBe107877	5 28 34.260	-67 13 25.90	15.23	0.21	90	20500 ±1200	3.4 ±0.2	208 ±15	319 ±10	B2III	c14
MHFBBe108272	5 28 32.127	-67 13 23.68	16.40	0.20	100	21500 ±1100	3.9 ±0.2	226 ±11	320 ±10	B2IV	c14
MHFBBe110827	5 27 28.582	-67 12 56.81	14.93	0.23	130	26500 ±1300	4.2 ±0.2	195 ±14	305 ±10	B1V	c17
MHFBBe116297	5 28 06.021	-67 11 47.44	16.14	0.16	110	23500 ±1200	4.0 ±0.2	226 ±11	319 ±10	B1V	
MHFBBe118313	5 26 55.945	-67 11 27.10	15.04	0.18	85	25000 ±1500	3.4 ±0.2	197 ±20	301 ±10	B1III	
MHFBBe118784	5 28 27.565	-67 11 28.50	14.79	0.18	185	27000 ±1400	3.4 ±0.2	388 ±19	296 ±10	B1III	
MHFBBe119521	5 30 35.252	-67 11 19.10	16.30	0.17	94	24000 ±1400	3.7 ±0.2	321 ±22	341 ±10	B1III	c11
MHFBBe132079	5 30 05.496	-67 8 53.45	16.24	0.20	80	25000 ±1500	4.4 ±0.3	318 ±32	305 ±10	B1V	
MHFBBe132205	5 29 25.872	-67 8 53.93	14.72	0.18	134	26000 ±1300	3.4 ±0.2	129 ±10	301 ±10	B1III	c18
MHFBBe136844	5 27 35.241	-67 7 54.44	15.15	0.19	110	23000 ±1200	3.5 ±0.2	348 ±17	315 ±10	B1III-IV	
MHFBBe137325	5 29 07.009	-67 7 49.28	16.30	0.16	110	15000 ±800	3.1 ±0.2	252 ±13	320 ±10	B5III	
MHFBBe138610	5 30 00.332	-67 7 44.02	14.82	0.17	129	25000 ±1200	3.7 ±0.2	171 ±10	314 ±10	B1IV	c16
MHFBBe140012	5 28 13.281	-67 7 20.77	14.94	0.18	130	23000 ±1200	3.5 ±0.2	246 ±12	297 ±10	B1.5III	c13
MHFBBe155603	5 28 47.760	-67 4 25.70	14.72	0.20	100	25000 ±1300	3.4 ±0.2	249 ±12	308 ±10	B1III	

Table 8. Stellar parameters of the LMC Be stars corrected for the effects of fast rotation assuming different rotation rates (Ω/Ω_c). The probably most suitable corrections are those corresponding to $\Omega/\Omega_c = 85\%$. The units are K for T_{eff}^o , dex for $\log g_o$, and km s^{-1} for $V\sin i^{\text{true}}$.

Star	$\Omega/\Omega_c = 85\%$			$\Omega/\Omega_c = 90\%$			$\Omega/\Omega_c = 95\%$		
	T_{eff}^o	$\log g_o$	$V\sin i^{\text{true}}$	T_{eff}^o	$\log g_o$	$V\sin i^{\text{true}}$	T_{eff}^o	$\log g_o$	$V\sin i^{\text{true}}$
KWBBe0044	23000±1100	3.2±0.2	119±10	23390±1100	3.3±0.2	121±10	23300±1100	3.3±0.2	121±10
KWBBe0075	24000±1400	3.6±0.2	193±13	24450±1400	3.6±0.2	195±13	23950±1400	3.6±0.2	198±13
KWBBe0091	21000±1000	3.4±0.2	211±10	21175±1000	3.4±0.2	211±10	21310±1000	3.5±0.2	217±10
KWBBe0152	25500±1200	3.8±0.2	394±19	25900±1200	3.8±0.2	388±19	25490±1200	3.8±0.2	400±19
KWBBe0171	24500±1200	3.8±0.2	275±14	24180±1200	3.9±0.2	277±14	24155±1200	3.8±0.2	284±14
KWBBe0177	33500±1800	3.9±0.2	508±50	33400±1800	3.9±0.2	516±50	33740±1800	4.0±0.2	527±50
KWBBe0203	25500±1500	3.6±0.2	268±25	26350±1500	3.5±0.2	268±25	25970±1500	3.5±0.2	269±25
KWBBe0276	23500±1100	3.5±0.2	253±12	23360±1100	3.5±0.2	257±12	23120±1100	3.5±0.2	261±12
KWBBe0287	21000±1200	3.4±0.2	230±15	21190±1200	3.5±0.2	234±15	21250±1200	3.5±0.2	237±15
KWBBe0323	25000±1400	3.9±0.2	282±19	24535±1400	3.9±0.2	281±19	24610±1400	3.9±0.2	283±19
KWBBe0342	24000±1400	4.3±0.2	316±31	23450±1400	4.3±0.2	322±31	24545±1400	4.3±0.2	321±31
KWBBe0344	23500±1100	4.0±0.2	225±11	23450±1100	4.0±0.2	225±11	23370±1100	4.0±0.2	228±11
KWBBe0347	25000±1300	3.8±0.2	344±23	25240±1300	3.8±0.2	343±23	25470±1300	3.9±0.2	349±23
KWBBe0374	24000±2200	4.3±0.4	345±54	23880±2200	4.3±0.4	347±54	24080±2200	4.4±0.4	352±54
KWBBe0579	20500±2300	3.8±0.4	320±50	21000±2300	3.9±0.4	323±50	21060±2300	3.9±0.4	332±50
KWBBe0622	18000±1600	4.0±0.3	315±48	17240±1600	3.9±0.3	314±48	17700±1600	3.9±0.3	335±48
KWBBe0624	22000±2400	3.8±0.3	356±55	22690±2400	3.8±0.3	353±55	22880±2400	3.8±0.3	359±55
KWBBe0874	20000±2900	4.3±0.4	270±52	20380±2900	4.3±0.4	275±52	20610±2900	4.4±0.4	280±52
KWBBe1055	25000±2600	4.2±0.4	433±67	24600±2600	4.3±0.4	441±67	24710±2600	4.3±0.4	441±67
KWBBe1108	20500±2300	4.3±0.4	326±51	20860±2300	4.3±0.4	332±51	20970±2300	4.4±0.4	338±51
KWBBe1175	23000±4300	4.5±0.4	354±100	23030±4300	4.5±0.4	359±100	23260±4300	4.5±0.4	364±100
KWBBe1196	19000±2200	4.2±0.4	378±65	18980±2200	4.2±0.4	386±65	19120±2200	4.2±0.4	394±65
MHFBe55075	23000±2600	3.9±0.4	274±43	23100±2600	4.0±0.4	276±43	23165±2600	4.0±0.4	282±43
MHFBe55920	24000±1400	4.1±0.2	129±12	23980±1400	4.1±0.2	128±12	23930±1400	4.1±0.2	129±12
MHFBe59721	19000±1100	4.2±0.2	208±18	19190±1100	4.2±0.2	212±18	19240±1100	4.2±0.2	214±18
MHFBe66252	28000±1500	4.3±0.2	459±45	27880±1500	4.3±0.2	465±45	28100±1500	4.4±0.2	473±45
MHFBe72704	23500±1100	3.6±0.2	114±10	23380±1100	3.6±0.2	117±10	23370±1100	3.6±0.2	117±10
MHFBe73013	27000±1200	4.6±0.2	411±20	27100±1200	4.6±0.2	422±20	27250±1200	4.6±0.2	422±20
MHFBe77796	26500±1500	3.7±0.2	126±10	26050±1500	3.7±0.2	130±10	26060±1500	3.7±0.2	129±10
MHFBe85028	24500±1200	4.0±0.2	277±13	24240±1200	4.0±0.2	279±13	24350±1200	4.0±0.2	282±13
MHFBe101350	25500±1200	3.9±0.2	230±11	25270±1200	3.9±0.2	232±11	25475±1200	3.9±0.2	234±11
MHFBe103914	29000±1300	3.8±0.2	382±18	27270±1300	3.6±0.2	385±18	28930±1300	3.8±0.2	394±18
MHFBe107771	20000±1100	4.0±0.2	331±29	19680±1100	4.0±0.2	333±29	19890±1100	4.0±0.2	341±29
MHFBe107877	22000±1200	3.6±0.2	216±15	22040±1200	3.7±0.2	219±15	22130±1200	3.7±0.2	222±15
MHFBe108272	22500±1100	4.1±0.2	235±11	22420±1100	4.1±0.2	236±11	22550±1100	4.1±0.2	237±11
MHFBe110827	27000±1300	4.3±0.2	201±14	26620±1300	4.3±0.2	205±14	27400±1300	4.3±0.2	205±14
MHFBe116297	25000±1200	4.1±0.2	233±11	24310±1200	4.1±0.2	234±11	24310±1200	4.1±0.2	237±11
MHFBe118313	26000±1500	3.5±0.2	207±20	26380±1500	3.6±0.2	208±20	27060±1500	3.6±0.2	209±20
MHFBe118784	30000±1400	3.8±0.2	404±19	28400±1400	3.7±0.2	406±19	30470±1400	3.8±0.2	416±19
MHFBe119521	25500±1400	4.0±0.2	330±22	24370±1400	3.9±0.2	334±22	25830±1400	4.0±0.2	337±22
MHFBe132079	25500±1500	4.5±0.3	326±32	26985±1500	4.6±0.3	335±32	26495±1500	4.6±0.3	332±32
MHFBe132205	27000±1300	3.6±0.2	137±10	26950±1300	3.6±0.2	136±10	28145±1300	3.7±0.2	139±10
MHFBe136844	25500±1200	3.8±0.2	360±17	26240±1200	3.9±0.2	362±17	25320±1200	3.8±0.2	365±17
MHFBe137325	17000±800	3.4±0.2	263±13	16550±800	3.5±0.2	271±13	16330±800	3.4±0.2	276±13
MHFBe138610	25500±1200	3.8±0.2	178±10	25210±1200	3.8±0.2	181±10	25560±1200	3.8±0.2	183±10
MHFBe140012	24500±1200	3.7±0.2	252±12	24400±1200	3.7±0.2	254±12	24470±1200	3.7±0.2	257±12
MHFBe155603	26600±1300	3.5±0.2	261±12	27220±1300	3.6±0.2	261±12	27525±1300	3.6±0.2	263±12

or older than $\log(t) = 7$ in their sample. We obtained that for $\log(t) \leq 7$ the fraction of Be stars is $\frac{Be}{all} = 4.8\%$, whereas for $\log(t) > 7$, $\frac{Be}{all} = 22\%$. Thus, the high proportion of Be stars in the clusters with $\log(t) > 7$ and their high rotational velocities may explain the discrepancy between the observed and predicted $V\sin i$ for a $12 M_{\odot}$ star of the same clusters. The high proportion of Be stars found in clusters with $\log(t) > 7$ is also

in agreement with results by Fabregat & Torrejón (2000), who found that Be stars reached the maximum abundance between 13 and 25 Myr.

Another explanation is related to the mass function of the sample stars of GH04. They used the prediction in rotational velocity across the main sequence for a $12 M_{\odot}$. However, the behaviour in $V\sin i$ during evolution is not identical for a $12 M_{\odot}$

Table 9. Apparent parameters $\log(L/L_\odot)$, M/M_\odot , and R/R_\odot interpolated or calculated for the sample of Be stars from HR diagrams taken from Charbonnel et al. (1993).

Star	$\log(L/L_\odot)$	M/M_\odot	R/R_\odot	Star	$\log(L/L_\odot)$	M/M_\odot	R/R_\odot
KWBBe0044	4.9±0.3	16.8±1.0	18.0±2.0	MHFBe59721	3.2±0.3	5.6±0.5	4.0±0.5
KWBBe0075	4.5±0.3	12.3±1.0	11.0±1.5	MHFBe66252	4.0±0.3	10.1±1.0	5.4±1.0
KWBBe0091	4.4±0.3	11.7±1.0	14.1±1.5	MHFBe72704	4.4±0.3	11.3±1.0	10.1±1.0
KWBBe0152	4.5±0.3	12.9±1.0	12.2±1.5	MHFBe73013	3.5±0.3	8.3±0.5	3.3±0.5
KWBBe0171	4.2±0.3	10.3±1.0	8.1±1.0	MHFBe77796	4.4±0.3	12.4±1.0	8.5±1.0
KWBBe0177	5.2±0.3	24.4±2.0	14.5±1.5	MHFBe85028	4.0±0.3	9.6±0.5	6.5±1.0
KWBBe0203	4.6±0.3	13.6±1.0	10.3±1.5	MHFBe101350	4.2±0.3	11.0±1.0	7.1±1.0
KWBBe0276	4.5±0.3	12.8±1.0	13.5±1.5	MHFBe103914	4.9±0.3	16.8±1.0	13.0±1.5
KWBBe0287	4.3±0.3	10.6±1.0	10.8±1.5	MHFBe107771	3.6±0.3	6.7±0.5	6.9±1.0
KWBBe0323	4.2±0.3	10.5±1.0	7.4±1.0	MHFBe107877	4.2±0.3	10.1±1.0	10.5±1.5
KWBBe0342	3.6±0.3	7.9±0.5	4.2±0.5	MHFBe108272	3.7±0.3	7.7±0.5	5.0±0.5
KWBBe0344	3.9±0.3	8.8±0.5	6.0±1.0	MHFBe110827	3.8±0.3	9.7±0.5	3.9±0.5
KWBBe0347	4.4±0.3	11.4±1.0	10.8±1.5	MHFBe116297	3.8±0.3	8.8±0.5	5.1±0.5
KWBBe0374	3.6±0.3	7.5±0.5	4.1±0.5	MHFBe118313	4.8±0.3	15.6±1.0	13.6±1.5
KWBBe0579	3.9±0.3	8.1±0.5	8.7±1.0	MHFBe118784	5.0±0.3	18.6±1.0	14.4±1.5
KWBBe0622	3.4±0.3	5.9±0.5	7.1±1.0	MHFBe119521	4.2±0.3	10.7±1.0	7.8±1.0
KWBBe0624	4.2±0.3	9.9±0.5	11.3±1.5	MHFBe132079	3.5±0.3	8.2±0.5	3.1±0.5
KWBBe0874	3.2±0.3	5.8±0.5	3.7±0.5	MHFBe132205	4.8±0.3	16.3±1.0	13.0±1.5
KWBBe1055	3.8±0.3	8.2±0.5	5.3±1.0	MHFBe136844	4.4±0.3	11.7±1.0	10.5±1.5
KWBBe1108	3.3±0.3	6.0±0.5	4.0±0.5	MHFBe137325	3.8±0.3	7.4±0.5	12.6±1.5
KWBBe1175	3.3±0.3	6.5±0.5	3.3±0.5	MHFBe138610	4.3±0.3	11.6±1.0	7.9±1.0
KWBBe1196	3.3±0.3	5.6±0.5	5.2±1.0	MHFBe140012	4.4±0.3	11.5±1.0	10.0±1.0
MHFBe55075	3.9±0.3	8.2±0.5	6.3±1.0	MHFBe155603	4.9±0.3	16.7±1.0	14.3±1.5
MHFBe55920	3.8±0.3	8.7±0.5	4.9±0.5				

and a $7 M_\odot$ star. In the latter case, following Meynet & Maeder (2000), the mass loss is much weaker than for massive stars ($M \geq 10 M_\odot$) and the evolutionary track presents an increase of velocity instead of a decrease. This may explain why B-type stars are more likely to increase their rotational velocity during their MS life than the more massive O-type stars.

5.2. Results for the LMC and comparison with the MW

In the following sub-sections we compare the obtained apparent fundamental parameters to previous studies, which generally did not take fast rotation effects into account in the determination of fundamental parameters.

For all stars in the LMC stellar sample studied in this paper, we find the following mean $V \sin i$ (in km s^{-1}) for B and Be stars in the field and clusters, where the given errors are the mean errors and the number in brackets is the number of stars used in the average:

$$\begin{aligned}
 \text{Be}_{\text{field+clusters}}: & \quad V \sin i = 272 \pm 20 (47), \\
 \text{B}_{\text{field+clusters}}: & \quad V \sin i = 119 \pm 20 (106) \\
 \text{Be}_{\text{field}}: & \quad V \sin i = 268 \pm 20 (27), \\
 \text{B}_{\text{field}}: & \quad V \sin i = 117 \pm 20 (93), \\
 (\text{B+Be})_{\text{clusters}}: & \quad V \sin i = 223 \pm 20 (33), \\
 \text{Be}_{\text{clusters}}: & \quad V \sin i = 278 \pm 20 (20), \\
 \text{B}_{\text{clusters}}: & \quad V \sin i = 140 \pm 20 (13).
 \end{aligned}$$

These mean $V \sin i$ values cannot be compared directly with values in the MW, because they are affected by ages and evolution, mass function of samples, etc. We must therefore select B and Be stars in the same range of spectral types and luminosity classes or of masses (when they are known) and ages for

samples in the LMC and in the MW. Then, to investigate the effect of metallicity and age on the rotational velocity, we first compare the mean $V \sin i$ of the B and Be stars in the LMC to the ones in the MW.

We calculate rotational velocities evolutionary tracks for different initial velocities and for a $7 M_\odot$ star, which corresponds to the maximum of the mass function for the B-type stars sample. We have obtained these curves by interpolation thanks to the Figure 5 published in Meynet & Maeder (2002) for the tracks of a $7 M_\odot$ with an initial velocity at the ZAMS = 300 km s^{-1} . And we have used the Figure 12 published in Meynet & Maeder (2000), and more particularly the Figure 5 from Maeder & Meynet (2001) in order to obtain tracks for different initial rotational velocities ($V_0 = 100, 200, 300, 400, 500 \text{ km s}^{-1}$). The use of tracks with a metallicity $Z = 0.00001$ for a $7 M_\odot$ is justified because the tracks for a star with $9 M_\odot$ at metallicity $Z = 0.004$ or $Z = 0.00001$ are quasi identical, then we expect that the tracks for a $7 M_\odot$ are identical at $Z = 0.00001$ and at $Z = 0.004$.

Let us note that due to fast internal angular momentum redistribution in the first $\approx 10^4$ years in the ZAMS, the surface rotational velocities decrease 0.8 times their initial value. Then, for the comparison sake with our observational data, the values plotted are not V but are average $V \sin i = (\pi/4)V$ (see eq. 1). For example, for an initial rotational velocity equals to 300 km s^{-1} , the angular momentum redistribution leads roughly to $V_{\text{ZAMS}} = 240 \text{ km s}^{-1}$, which corresponds to $V \sin i = (\pi/4) \times 240 \approx 190 \text{ km s}^{-1}$. The curves are only slightly affected by mass loss effects. Due to the low metallicity LMC environment, the mass-loss dependent effects are even less noticeable.

Table 10. Comparison of mean rotational velocities for B and Be stars with spectral types B1-B3 and luminosity classes from V to III in the LMC and the MW. The values in brackets represent the number of stars in the samples.

	Field B stars	Field Be stars	Clusters B stars	Clusters Be stars
LMC this study	121 ± 10 (81)	268 ± 30 (26)	144 ± 20 (10)	266 ± 30 (19)
LMC Keller (2004)	112 ± 50 (51)		146 ± 50 (49)	
MW Glebocki et al. (2000)	124 ± 10 (449)	204 ± 20 (48)		
MW Levato et al. (2004)	108 ± 10 (150)			
MW Yudin (2001)		207 ± 30 (254)		
MW Chauville et al. (2001)		231 ± 20 (56)		
MW WEBDA $\log(t) < 7$			127 ± 20 (44)	199 ± 20 (8)
MW WEBDA $\log(t) > 7$			149 ± 20 (59)	208 ± 20 (45)

Table 11. Results of the Student’s t-test comparisons of the mean rotational velocities for B and Be stars with spectral types B1-B3 and luminosity classes from V to III in the LMC and the MW. The first column gives the compared studies, the 2nd column gives the result of the test, the 3rd column gives the α coefficient and the 4th column gives the probability of differences ‘P’. The last column gives a comment about the result according to the convention. The comment “limit” means that the number of stars in samples is low and the value of mean $V\sin i$ may be affected by the distribution of the inclination angles.

Comparison	result	α	P	comment
Be				
Be LMC field/ Be MW Glebocki et al. (2000)	10.81	0.05	90-95 %	significant difference
Be LMC field/ Be MW Yudin (2001)	9.84	0.05	90-95%	significant difference
Be LMC field/ Be MW Chauville et al. (2001)	6.52	0.05	90-95%	significant difference
Be LMC clusters/ Be MW WEBDA $\log(t) < 7$	5.58	0.1	80-90 %	limit, slight difference
Be LMC clusters/ Be MW WEBDA $\log(t) > 7$	8.91	0.05	90-95%	significant difference
Be MW WEBDA $\log(t) < 7$ / Be MW WEBDA $\log(t) > 7$	1.15	0.3	50-70%	limit, no significant difference
B				
B LMC field/ B LMC field Keller (2004)	1.56	0.3	50-70%	no significant difference
B LMC field/ B MW Glebocki et al. (2000)	2.48	0.2	70-80%	no significant difference
B LMC field/B MW Levato et al. (2004)	9.4	0.05	90-95%	significant difference
B LMC clusters/ B LMC clusters Keller (2004)	0.12	0.9	<10%	limit, no difference
B LMC clusters/ B MW WEBDA $\log(t) < 7$	2.38	0.2	70-80%	limit, no significant difference
B LMC clusters/B MW WEBDA $\log(t) > 7$	0.72	0.5	10-50 %	limit, no difference
B MW WEBDA $\log(t) < 7$ /B MW WEBDA $\log(t) > 7$	5.47	0.1	80-90 %	slight difference
Fields / clusters				
Be LMC field/ Be LMC clusters	0.22	0.5	10-50 %	no difference
B LMC field/ B LMC clusters	5.88	0.1	80-90 %	limit, slight difference
Be MW Yudin (2001)/ Be MW WEBDA $\log(t) < 7$	0.70	0.5	10-50%	no difference
Be MW Yudin (2001)/ Be MW WEBDA $\log(t) > 7$	0.21	0.5	10-50%	no difference
B MW Glebocki et al. (2000)/ B MW WEBDA $\log(t) < 7$	1.68	0.3	50-70 %	no difference
B MW Glebocki et al. (2000)/ B MW WEBDA $\log(t) > 7$	15.50	0.02	95-98 %	significant difference

In the present work, the purpose of these curves is only to give a rough interpretation of the behavior observed of $\langle V\sin i \rangle$.

We determine the ages of stars of the field and of several clusters or associations in our observations. For this purpose, we use HR evolutionary tracks (for non-rotating stars) for the stars of the sample unaffected by rapid rotation and for Be stars corrected for the effects of fast rotation with $\Omega/\Omega_c = 85\%$. For the cluster NGC 2004, we obtain $\log(t) = 7.40$, which is close to the value obtained in previous studies: $\log(t) = 7.30$ (Keller 1999) and 7.40 (Maeder et al. 1999). This comparison validates our method to determine ages for clusters.

5.2.1. Field B and Be stars

The mean $V\sin i$ obtained for B stars in the field of the LMC closely agrees with Keller’s (2004) results in the same age range (see Table 10 and Fig. 10, upper panel). To compare the rotational velocity of B stars in the LMC with the MW, we use the studies of Levato & Grosso (2004) and Glebocki & Stawikowski (2000). In these studies, we select stars with spectral types ranging from B1 to B3 and luminosity classes from V to III, because ages and masses were not determined. To compare the rotational velocity of Be stars in the LMC with the MW, we use Chauville et al. (2001), Glebocki & Stawikowski (2000) and Yudin (2001) with the same selection criteria as for B stars. The comparison of $V\sin i$ in the LMC and the MW for B and Be stars in the field is presented in Table 10 and Fig. 10,

upper panel. The range of stellar ages is reported as the dispersion in age in the figure. For samples with an unknown age, we adopt as error bar the duration of the Main Sequence for a $7 M_{\odot}$ star, which overestimates the age uncertainty. The curves in Fig. 10, upper panel, show the evolutionary tracks of rotational velocity during the Main Sequence for different initial velocity for a $7 M_{\odot}$ star, which corresponds to the maximum of the mass function of the B-stars sample.

In order to know if the samples contain a sufficient number of elements for the statistic to be relevant and give an average $V \sin i$ not biased by inclination effects, we calculate averages for samples with different number of elements. The deviation of the averages gives the statistical error. If this statistical error is smaller than the error on the data, the value determined for the data is statistically significant and does not represent an effect of inclination. Thanks to this test, we find that our samples in the LMC and in the MW are statistically significant even in the cases when the number of stars does not exceed 10. For example, in Table 10, we have found no difference between the cluster B stars ($V \sin i = 144 \text{ km s}^{-1}$, 10 stars) following our results and according to Keller (2004) ($V \sin i = 146 \text{ km s}^{-1}$, 49 stars).

We complete the statistical studies by a Student's t-test (see Table 11) in order to know whether the differences observed in the samples are significant. The Student test gives:

(i) for field B stars: There is no significant difference between the LMC studies carried-on in this paper and Keller's (2004). The test further gives no significant difference between LMC and MW studies, when the data used for the MW are those of Glebocki & Stawikowski (2000). There are, however, significant differences when the comparison is based on data taken from Levato & Grosso (2004). It is therefore difficult to conclude whether B stars have similar rotational velocities in the LMC and the MW fields.

(ii) for field Be stars: A significant difference between studies in the LMC (this paper) and the MW. Field Be stars in the LMC have a rotational velocity higher than in the MW.

5.2.2. B and Be stars in clusters

As for B stars in the field, we find that the mean $V \sin i$ of B stars in the LMC clusters ($\log(t) > 7$) determined from our observations closely agrees with Keller's (2004) results (see Table 10 and Fig. 10, lower panel). In the MW, we selected young clusters with $\log(t) < 8$ (some of them were observed by GH04) in the WEBDA database for which published $V \sin i$ and MK classification exist. We distinguish two groups: the younger clusters with $\log(t) < 7$ and older clusters with $\log(t) > 7$. The younger clusters (given by increasing age) are: IC 1805, Trumpler 14, IC 2944, NGC 6193, NGC 2362, NGC 2244, NGC 6611, NGC 2384, NGC 3293, and NGC 1502. The older clusters (given by increasing age) are: NGC 869, NGC 884, NGC 4755, IC 2395, NGC 7160, and NGC 2422. Their difference in age gives the age–dispersion reported in Fig 10, lower panel. The ages are those given by GH04 and in WEBDA.

The results concerning B stars in the LMC clusters and MW Be stars with $\log(t) < 7$ must be taken cautiously. In fact, the samples are not numerous enough to have the inclination angle effects, in $V \sin i$ averages, entirely removed so as to reflect the i/V_i -dependent information properly. For the stars in these clusters, the Student's t-test (see Table 11) gives:

(i) for B stars: A slight difference between younger ($\log(t) < 7$) and older ($\log(t) > 7$) clusters in the MW, which may be explained by the effect of evolution on rotational velocity, but no significant difference between the LMC and the MW clusters with $\log(t) > 7$. B stars in the LMC and MW clusters seem to have a similar rotational velocity when intervals of similar ages are compared.

(ii) for Be stars: A significant difference between the LMC and the MW clusters. Be stars in the LMC clusters have a rotational velocity higher than in the MW clusters. However, the number of Be stars observed in LMC clusters, as well as the number of Be stars identified in young MW clusters, is poor and may affect the statistics.

Fig. 10, lower panel, illustrates the comparison of the mean $V \sin i$ in the LMC and the MW for B and Be stars in clusters. As in Fig 10, upper panel, the curves show the evolutionary tracks of rotational velocity during the Main Sequence for different initial velocity for a $7 M_{\odot}$ star.

5.2.3. Comparison between field and clusters

Results on rotational velocity of B and Be stars in the field and clusters presented in Sect. 5.2.1 and 5.2.2 (see also Table 10 and Table 11) lead to the following conclusions:

(i) According to Meynet & Maeder (2000), the lower the mass-loss in massive stars is, the lower the metallicity is. We can expect that stars in low-metallicity regions may lose less angular momentum and then better preserve the initial high rotational rates. Such a metallicity effect seems to be present in Be stars, as we see that they rotate faster in the field and clusters of the LMC than in the MW. However, we were not able to detect such an effect in B stars.

(ii) Be stars rotate more rapidly than B stars in the field as well as in clusters, in the LMC, and the MW. Be stars would begin their life on the MS with an initial rotational velocity higher than the one of B stars. The lower the metallicity environment is, the higher the initial rotational velocity of Be stars would be. Moreover, we note that these objects would require an initial rotational velocity of at least $\sim 250 \text{ km s}^{-1}$.

(iii) No significant differences can be found between the rotational velocity of field and cluster Be stars, neither in the LMC nor in the MW.

(iv) No significant differences can be found between rotational velocities of young field and cluster B stars in the LMC and in the MW. However, there is a significant difference between the rotational velocity of older field and cluster B stars in the MW. This fact can be explained in terms of evolution of rotational velocities.

5.2.4. Be stars: mass and rotation

The number of Be stars is too low to make a statistical study by mass range on $V \sin i$ in clusters and in the field of the LMC separately. As mentioned in the previous section, we did not find significant differences in mean $V \sin i$ values for Be stars between clusters and the field. Therefore we compare Be stars only by intervals of mass, regardless of their location.

(i) for $5 < M < 10 M_{\odot}$, the sub-sample contains 21 stars. The determined mean parameters are: $\langle M \rangle = 7.7 M_{\odot}$, $\langle R \rangle = 5.8 R_{\odot}$, and $\langle V \sin i \rangle = 285 \text{ km s}^{-1}$, which correspond to a mean ratio $\Omega/\Omega_c \approx 85\% \pm 9\%$

(ii) for $10 < M < 12 M_{\odot}$, the sub-sample contains 13 stars. The determined mean parameters are: $\langle M \rangle = 11.0 M_{\odot}$, $\langle R \rangle = 9.3 R_{\odot}$, and $\langle V \sin i \rangle = 259 \text{ km s}^{-1}$, which correspond to a mean ratio $\Omega/\Omega_c \approx 83\% \pm 9\%$;

(iii) for $18 > M > 12 M_{\odot}$, the sub-sample contains 10 stars. The determined mean parameters are: $\langle M \rangle = 14.6 M_{\odot}$ close to $15 M_{\odot}$, $\langle R \rangle = 12.7 R_{\odot}$, and $\langle V \sin i \rangle = 224 \text{ km s}^{-1}$, which correspond to a mean ratio $\Omega/\Omega_c \approx 73\% \pm 9\%$.

These results are plotted in Fig. 11 and compared to the theoretical evolutionary tracks for a 7 and 15 M_{\odot} star for different values of initial rotational velocity (Maeder & Meynet 2001). These curves can be considered as envelopes of evolutionary tracks of our sample of Be stars in the LMC. This figure shows that stars follow the theoretical rotational velocity evolution in a low metallicity environment: the mean $V \sin i$ decreases as the mass increases. This trend can be explained by a difference in mass loss between massive and less massive stars.

5.2.5. Star formation conditions and magnetic field

According to Stepien (2002), the sufficient condition for a star to rotate rapidly on the ZAMS is the presence of a weak or moderate stellar magnetic field and the existence of an accretion disk for at least 10% of its pre-Main Sequence (PMS) phase. The magnetic field and its interactions with the disk or wind and other phenomena such as accretion have an impact on rotational velocity during the PMS and affect the initial rotational velocity (spin down for strong values of magnetic field) in the Main Sequence (MS). For stars in the MW, the progenitors of all Be stars would possess a fossil magnetic field with a surface intensity between 40 and 400 G and, due to the short PMS phase for the early types, they would conserve their strong rotational velocity during the MS. On the opposite, stars with a magnetic field stronger than 400 G would become slowly rotating magnetic B stars. In the LMC and other environments of low metallicity, the magnetic field has less braking impact on the velocity as explained by Penny et al. (2004) due to the lower abundances of metals. It may explain why Be stars in the LMC can rotate initially with higher velocities than in the MW, as shown in Fig. 10, upper panel. Note that a weak magnetic field is suspected in the classical Be star ω Ori (Neiner et al. 2003).

5.3. Evolutionary status of Be stars in the LMC

Using the same approach as the one described by Zorec et al. (2005), we studied the evolutionary status of the LMC Be stars in our sample. We used evolutionary tracks with an initial velocity $V_0 = 300 \text{ km s}^{-1}$ provided by Maeder & Meynet (2000). These evolutionary tracks for rotating stars are only available for stars in the MW. They show a slight shift towards lower temperatures and an extension of the time a star may spend on the MS (τ_{MS}), compared to evolutionary tracks of non-rotating stars. Therefore, a star placed in a HR diagram for non-rotating stars has a different age (τ) and a different evolutionary status $\frac{\tau}{\tau_{MS}}$ than if it would be placed in an HR diagram for rotating stars. Fig. 12 shows the evolutionary status of Be stars in the sample. It appears that more massive Be stars in our sample in the LMC seem to be evolved, since they are localized mainly in the second part of the MS. Contrary to previous similar studies (Zorec et al. 2005, Frémat et al. 2005), in our Be star sample, massive stars ($M \gtrsim 10 M_{\odot}$) by the end of the MS evolutionary phase represent a high fraction of the total number of the studied stars (60%). The distribution obtained cannot correspond only to differences in the mass-dependent evolutionary sampling, but it could reflect some star formation history in the region: stars with $M \gtrsim 10 M_{\odot}$ in $\tau/\tau_{MS} \gtrsim 0.5$ have an average age $\langle \tau \rangle \sim (1.5 \pm 0.4) \times 10^7 \text{ yr}$, stars with $M \lesssim 10 M_{\odot}$ in $\tau/\tau_{MS} \gtrsim 0.5$ have $\langle \tau \rangle \sim (2.9 \pm 0.2) \times 10^8 \text{ yr}$, while those with $M \lesssim 10 M_{\odot}$ and $\tau/\tau_{MS} \lesssim 0.5$ have $\langle \tau \rangle \sim (0.7 \pm 0.6) \times 10^7 \text{ yr}$.

The observed trend is only indicative, because evolutionary tracks for massive stars are mass loss dependent and the initial rotational velocities of Be stars are higher than 300 km s^{-1} . Nevertheless, according to Zorec et al. (2005), changes of initial velocities from $V_0 = 300 \text{ km s}^{-1}$ to higher values do not seem to strongly affect evolutionary tracks.

However, several Be stars with lower mass seem to be close to the ZAMS, which is inconsistent with the assumption that the Be star phenomenon occurs preferentially in the second half of the MS life. Those objects, for which spectra were mostly obtained with low S/N ratio, need to be reobserved to clearly confirm their fundamental parameters.

6. Conclusions

With the VLT-GIRAFFE spectrograph, we obtained spectra of a large sample of B and Be stars in the LMC-NGC 2004 and in its surrounding field. We determined fundamental parameters for B stars in the sample, and apparent and parent non-rotating counterpart (pnrc) fundamental parameters for fast rotators such as Be stars.

From the $V \sin i$ study for B and Be stars in the LMC and its comparison with the MW, we conclude that Be stars begin their life on the MS with a stronger initial velocity than B stars. Moreover, this initial velocity is sensitive to the metallicity. Consequently, only a fraction of B stars can become Be stars. This result may explain the differences in the proportion of Be stars in clusters with similar age.

Our results support Stepien's scenario (2002): massive stars with a weak or moderate magnetic field and with an accretion disk during at least 10% of their PMS lifetime would reach

the ZAMS with sufficiently high initial rotational velocity to become Be stars.

We find no clear influence of the metallicity on rotational velocity in B-type stars. The low metallicity may favour the PMS evolution of high velocity stars by minimizing the braking due to magnetic field interactions with the disk, but the influence of metallicity during the life of B-type stars in the MS is not preponderant. As Be stars are not critical rotators, an additional process, such as magnetic field by transferring momentum to the surface or non-radial pulsations (see Rivinius et al. 1998), must provide additional angular momentum to eject material from the star.

The effects of metallicity, the star formation conditions and the evolutionary status of B and Be stars discussed in this paper will be investigated in a forthcoming paper in the Small Magellanic Cloud, which has a lower metallicity than the Large Magellanic Cloud, in order to enlarge the results presented here.

Acknowledgements. We would like to thank Dr H. Flores for performing the observing run in November 2003 with success and good quality. We thank Drs M.R. Cioni and J. Smoker for their help during the observing run in April 2004. We also thank the referee Dr S. J. Smartt for his constructive remarks. This research has made use of the Simbad database and Vizier database maintained at CDS, Strasbourg, France, as well as of the WEBDA database.

References

- Azzopardi, M. 1987, A&AS, 69, 421
 Ballereau, D., Zorec, J. & Chauville, J. 1995, A&AS, 111, 423
 Bica, E.L.D., Geisler, D., Dottori, H., et al. 1998, AJ, 116,723
 Bouret, J. C., Lanz, T., Hillier, D. J., et al. 2003, AJ, 595, 1182
 Castelli, F., Gratton, R. G., & Kurucz, R. L. 1997, A&A, 318, 841
 Charbonnel, C., Meynet, G., Maeder, A., et al. 1993, A&AS, 101, 415
 Chauville, J., Zorec, J., Ballereau, D., et al. 2001, A&A, 378, 861
 Cunto, W., Mendoza, C., Ochsenbein, F., & Zeippen, C. J. 1993, A&A, 275, L5
 Didelon, P. 1982, A&ASS, 50, 199
 Fabregat, J. & Torrejón, J. M. 2000, A&A, 357, 451
 Frémat, Y., Neiner, C., Hubert, A.-M. et al. 2005a, A&A, in press, [astroph/0509336](#)
 Frémat, Y., Zorec, J., Hubert, A.-M. & Floquet, M. 2005b, A&A, 440, 305
 Gies, D. R. & Huang, W. 2004, IAUS, 215, 57 (GH04)
 Glebocki, R. & Stawikowski, A. 2000, Acta Ast., 50, 509
 Gray, R. O. & Corbally, C. J. 1994, AJ, 107, 742
 Hillier, D.J. & Miller, D.L. 1998, ApJ, 496, 407
 Hubeny, I. & Lanz, T. 1995, ApJ, 439, 875
 Jaschek, C. & Jaschek, M. 1995, Cambridge University Press, The behavior of chemical elements in stars
 Keller, S.C. 1999, AJ, 118, 889
 Keller, S.C. 2004, PASA, 21, 310
 Keller, S.C., Wood, P.R. & Bessell, M.S. 1999, A&AS, 134, 489
 Korn, A.J., Keller, S.C., Kaufer, A., et al. 2002, A&A, 385, 143
 Kurucz, R. L. 1993, Kurucz CE-ROM No.13. Cambridge, Mass.: Smithsonian Astrophysical Observatory.
 Lanz, T. & Hubeny, I. 2003, ApJS, 146, 417
 Levato, H. & Grosso, M. 2004, IAUS, 215, 51
 Martayan, C., Hubert, A.-M., Floquet, M., et al. 2005, A&A, in press, [astroph0509339](#)
 Maeder, A., Grebel, E.K. & Mermilliod, J.C. 1999, A&A, 346, 459
 Maeder, A. & Meynet, G. 2000, ARAA, 38, 143
 Maeder, A. & Meynet, G. 2001, A&A, 373, 555
 Meynet, G. & Maeder, A. 2000, A&A, 361, 101
 Meynet, G. & Maeder, A. 2002, A&A, 390, 561
 Neiner, C., Hubert, A.-M., Frémat, Y., et al. 2003, A&A, 409, 275
 Penny, L. R., Sprague, A. J., Seago, G., et al. 2004, ApJ, 617, 1316
 Rivinius, Th., Baade, D., Stefl, S., et al. 1998, BeSN, 33, 15
 Rolleston, W. R. J., Brown, P. J. F., Dufton, P. F., Howarth, I. D. 1996, A&A, 315, 95
 Royer, F., Melo, C., Mermilliod, J.-C., et al. 2004, IAUS, 215, 71
 Sigut, T. A. A. 1996, ApJ, 473, 452
 Stepién, K. 2002, A&A, 383, 218
 Varosi, F., Lanz, T., deKoter, A., et al. 1995, <ftp://idlastro.gsfc.nasa.gov/pub/contrib/varosi/modion>
 Yudin, R. V. 2001, A&A, 368, 912
 Zorec, J., Frémat, Y. & Cidale, L. 2005, A&A, 441, 235
 Zorec, J. 1986, PhD Thesis: Structure et rotation différentielle dans les étoiles B avec et sans émission (Paris: Université VII, 1986)

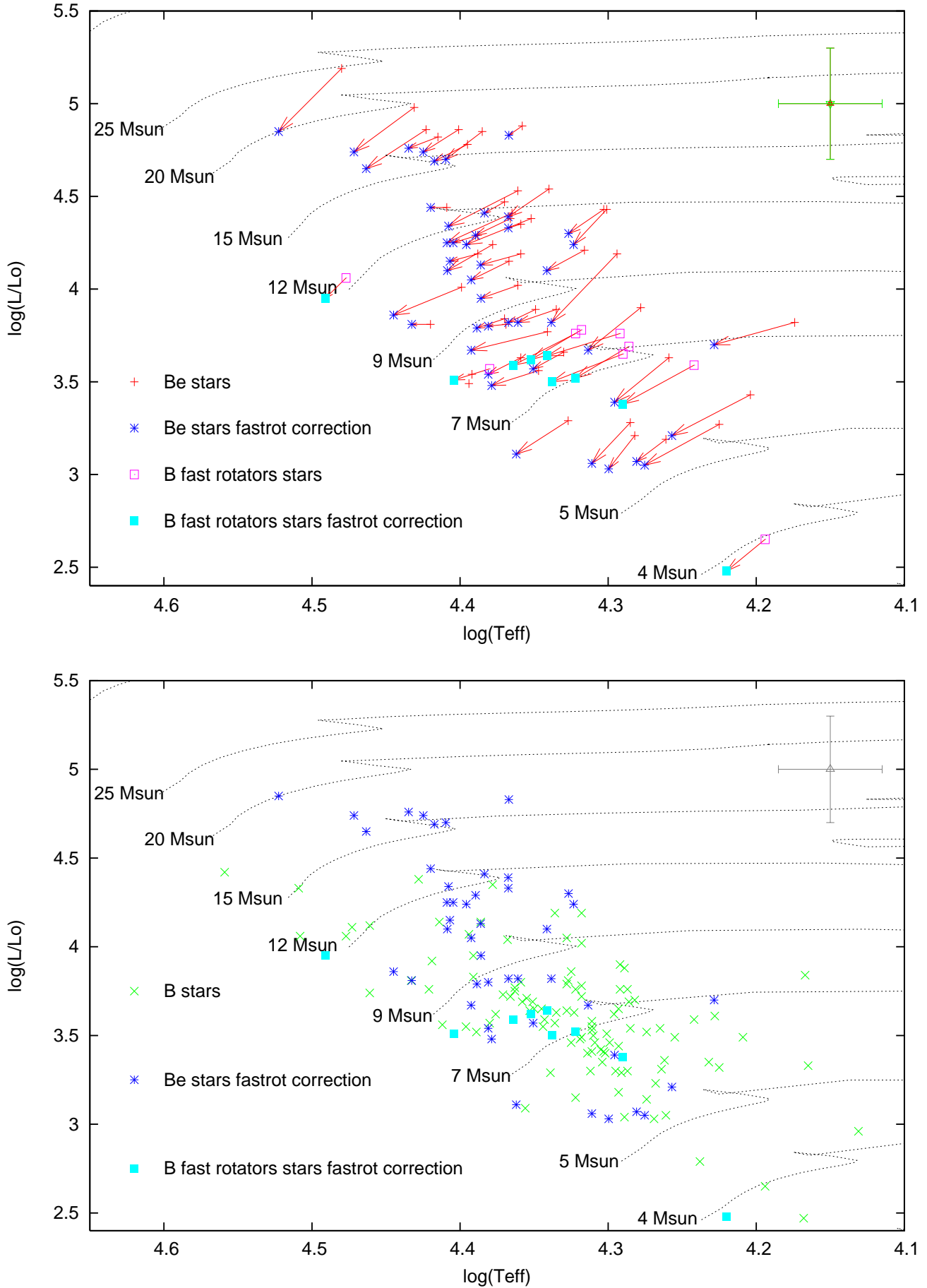


Fig. 5. HR diagrams for the studied B stars, including rapid rotators, and Be stars. Top: The effects of fast rotation are taken into account with $\Omega/\Omega_c = 85\%$ for Be stars and rapidly rotating B stars. Bottom: B stars and fast rotators (Be and B stars) corrected for their fast rotation. Common: The adopted metallicity for the LMC comes from Korn et al. (2002), Rolleston et al. (1996). Green 'x' represent B stars, red '+' represent Be stars with their apparent parameters, and blue '*' Be stars corrected with FASTROT with $\Omega/\Omega_c = 85\%$. Pink empty squares represent rapidly rotating B stars with their apparent parameters, and filled blue squares,

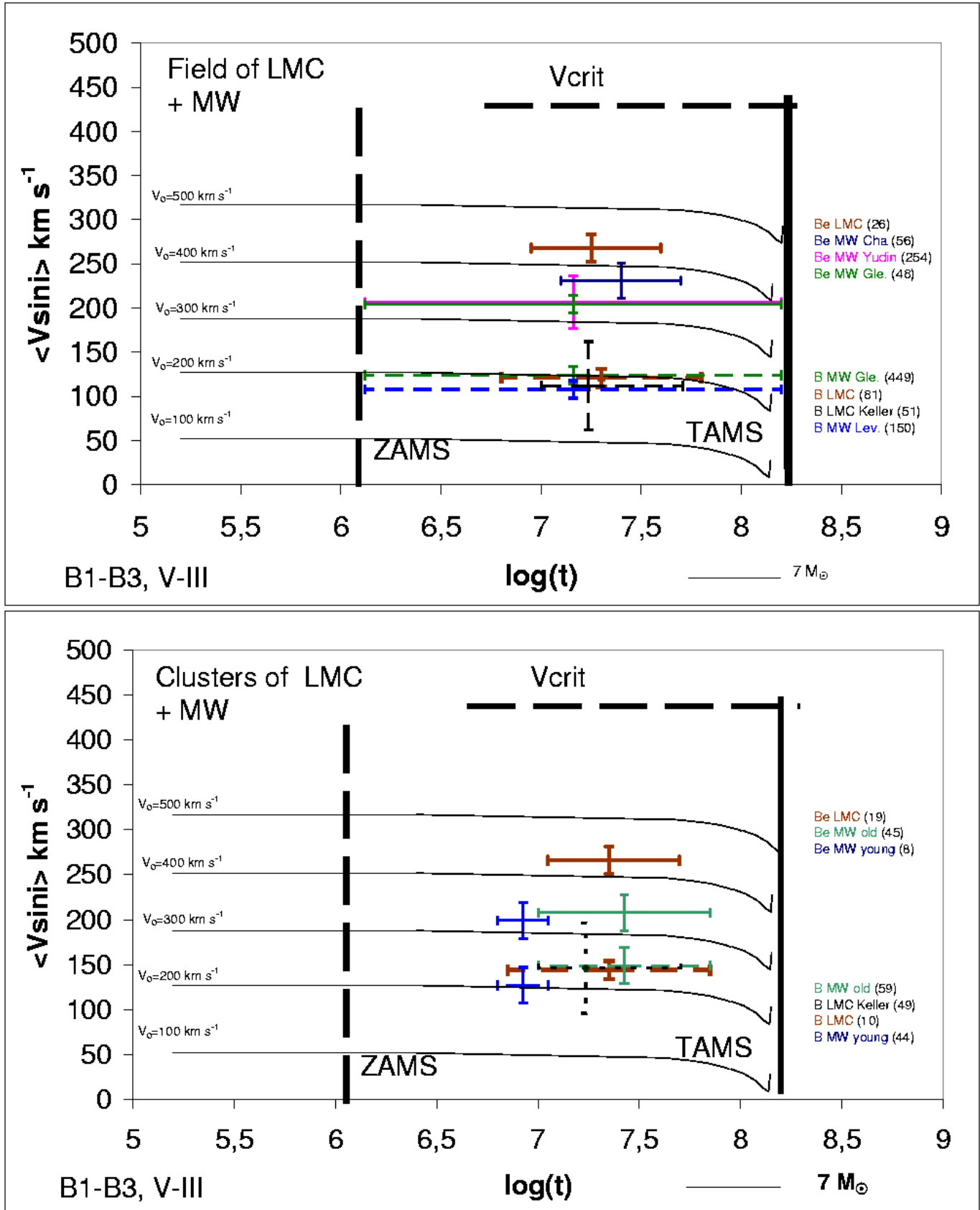


Fig. 10. Top: Comparison of mean $V \sin i$ in the LMC and the MW for field B and Be stars. Evolutionary tracks of rotational velocity during the Main Sequence life are given for different initial velocities for a $7 M_{\odot}$ star. The ZAMS and TAMS are indicated by vertical lines and the critical $V \sin i$ by a horizontal dotted line. The number of stars for each study is given in brackets. The dispersion in ages corresponds to the range of individual stellar ages in the samples, when these ages are known, or to the Main Sequence lifetime. The considered studies are: for the LMC, this paper and Keller (2004); for the MW, Cha = Chauville et al. (2001), Yudin (2001), Gle = Glebocki & Stawikowski (2000), and Lev = Levato & Grosso (2004). Bottom: same figure but for clusters. The considered studies are: for the LMC, this paper and Keller (2004), and for the clusters in the MW, the WEBDA database.

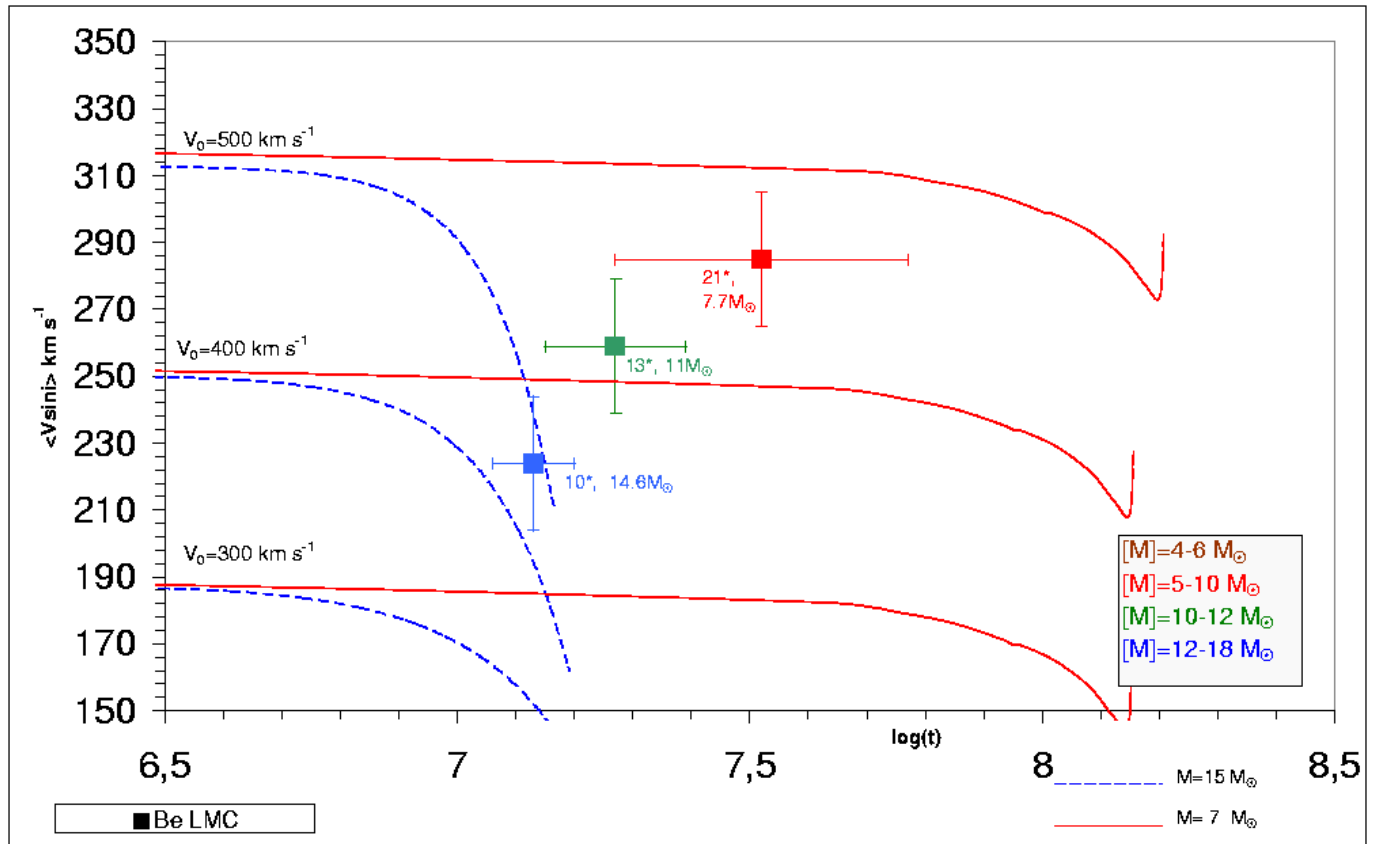


Fig. 11. Comparison of mean $V \sin i$ for Be stars in the study for three different intervals of masses: $5M_\odot < M < 10M_\odot$, $10M_\odot < M < 12M_\odot$ and $12M_\odot < M < 18M_\odot$. The numbers given, towards the crosses, are the number of stars and the mean mass. The curves show the evolutionary tracks of rotational velocity during the Main Sequence for different initial velocity for stars with $7 M_\odot$ (solid curve) and $15 M_\odot$ (dotted curve). The dispersion in ages corresponds to the range of individual stellar ages in the sub-samples.

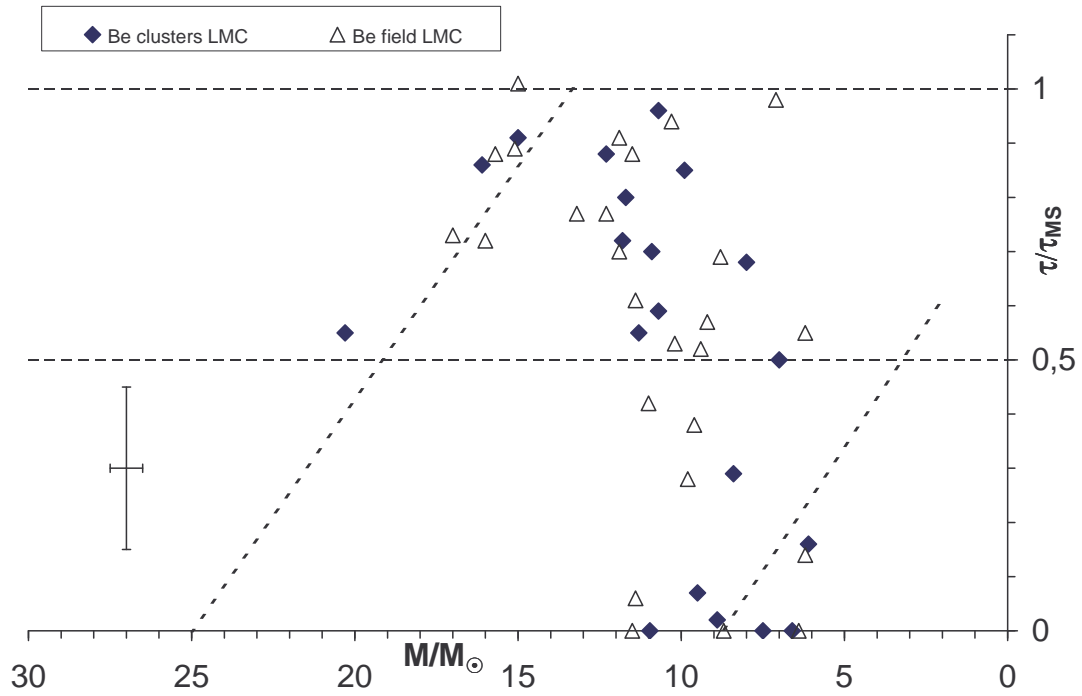


Fig. 12. Evolutionary status of Be stars in the sample. The parameters of Be stars are corrected with FASTROT with $\Omega/\Omega_c = 85\%$ and ages are determined in HR diagrams with $V_0 = 300 \text{ km s}^{-1}$. The typical errors are shown in the lower left corner. The dotted diagonals, which show the area of existing Be stars in the Milky Way, come from Zorec et al. (2005).